Transilvania
University
of Brasov

INTERDISCIPLINARY DOCTORAL SCHOOL

Faculty of Materials Science and Engineering

Ing. Alonso Molledo GORKA

Nucleation and Growth of Graphite in Cast Iron

Germinarea și creșterea grafitului în fonte

ABSTRACT /REZUMAT

Scientific supervisor

Prof. dr. ing. Aurel CRIȘAN

Transilvania University of Brasov

BRAȘOV, 2019

To Mrs/Mr.....

Reviewing board of the doctoral thesis

Enforced by the Decision of the Rector of the Transilvania University of Brașov

Nr. 9952 from 04.07.2019

PRESIDENT:	**Prof. Dr. Ing. Machedon Pisu Teodor** **Transilvania University of Brasov**
SCIENTIFIC SUPERVISOR:	**Prof. Dr. Ing. Crișan Aurel** **Transilvania University of Brasov**
OFFICIAL REVIEWERS:	**Prof. Dr. Ing. Ștefănescu Doru** **The Ohio State University- USA**
	Prof. Dr. Ing. Ripoșan Iulian **Polytechnic University of Bucharest**
	Prof. Dr. Ing. Chișamera Mihai **Polytechnic University of Bucharest**

Date, time and place of the public defence of the doctoral thesis: 26.09.2019; at 11,00; room W III 4.

Please send us, in time, your eventual comments, appreciations or observations on the content of this thesis, by mail on the following address galonso@azterlan.es

Also, we would like to invite you to take part in the public session of the thesis' defense.

Thank you!

CONTENT

1. INTRODUCTION 1

2. FUNDAMENTALS OF SOLIDIFICATION OF CAST IRON 4

2.1. PROCESS OF NUCLEATION 4

2.1.1. CONDITIONS FOR GRAPHIT CRYSTALLIZATION 4

2.2. NUCLEATION OF GRAPHITE 6

2.2.1. NUCLEATION OF LAMELLAR GRAPHITE 7

2.2.2. NUCLEATION OF COMPACTED GRAPHITE 7

2.2.3. NUCLEATION OF SPHERODIAL GRAPHITE 8

2.3. GROWTH OF GRAPHITE 9

2.3.1. SOLIDIFICATION OF LAMELLAR GRAPHITE (LG) 10

2.3.2. SOLIDIFICATION OF COMPACTED GRAPHITE (CG) 10

2.3.3. SOLIDIFICATION OF SPHERODIAL GRAPHITE (SG) 11

3. OBJECTIVES 13

4. THEORETICAL CONTRIBUTION 14

4.1. ELLINGHAM'S DIAGRAMS 14

4.2. DISREGISTRY CALCULATIONS 17

4.2.1. CALCULATION OF GRAPHITE/TiC DISREGISTRY 17

4.2.2. CALCULATION OF GRAPHITE/TiN DISREGISTRY 17

4.2.3. CALCULATION OF GRAPHITE/(Mg-Si-Al) NITRIDES DISREGISTRY 18

5. RESEARCH METHODOLOGY 20

5.1. EXPERIMENTAL STRATEGY 20

5.2. EXPERIMENTAL RESULTS. LAMELLAR GRAPHITE 21

5.2.1. INFLUENCE OF THE ADDITION OF SULFUR 26

5.2.2. INFLUENCE OF THE ADDITION OF TITANIUM 27

5.2.3. INFLUENCE OF THE NUCLEI ON THE GROWTH OF GRAPHITE 27

5.3. EXPERIMENTAL RESULTS. TADPOLE GRAPHITE 28

5.4. EXPERIMENTAL RESULTS. COMPACTED GRAPHITE 31

5.4.1. EFFECT OF THE ADDITION OF TITANIUM IN THE BASE METAL 35

5.4.2. EFFECT OF THE INOCULATION PROCESS 38

5.4.2.1. Ce inoculant 38

5.4.2.2. MnZr inoculant 39

5.4.3. EFFECT OF THE QUENCHING TIME 39

5.4.4. INFLUENCE OF THE NUCLEI IN THE GROWTH OF GRAPHITE 40

5.5. EXPERIMENTAL RESULTS. SPHEROIDAL GRAPHITE 41

5.5.1. EFFECT OF THE ADDITION OF TITANIUM IN THE BASE METAL 44

5.5.2. EFFECT OF THE INOCULATION PROCESS 49

5.5.2.1. Ti inoculant 50

5.5.2.2. Ba inoculant 50

5.5.2.3. Ce inoculant 50

5.5.2.4. ZrMn inoculant 51

5.5.3. EFFECT OF THE QUENCHING TIME 51

5.5.4. INFLUENCE OF THE NUCLEI IN THE GROWTH OF GRAPHITE 52

6. FINAL CONCLUSIONS 54

7. ORIGINAL CONTRIBUTIONS AND FUTURE RESEARCH DIRECTION 56

8. REFERENCES 58

CUPRINS

1. INTRODUCERE 1

2. PRINCIPIILE FUNDAMENTALE ALE SOLIDIFICĂRII FONTEI 4

2.1. PROCESUL DE GERMINARE 4

2.1.1. CONDIȚII PENTRU CRISTALIZAREA GRAFITULUI 4

2.2. GERMINAREA GRAFITULUI 6

2.2.1. GERMINAREA GRAFITULUI LAMELAR 7

2.2.2. GERMINAREA GRAFITULUI COMPACTIZAT 7

2.2.3. GERMINAREA GRAFITULUI SFEROIDAL 8

2.3. CREȘTEREA GRAFITULUI 9

2.3.1. SOLIDIFICAREA GRAFITULUI LAMELAR (LG) 10

2.3.2. SOLIDIFICAREA GRAFITULUI COMPACTIZAT (CG) 10

2.3.3. SOLIDIFICAREA GRAFITULUI SFEROIDAL (SG) 11

3. OBIECTIVE 13

4. CONTRIBUȚIE TEORETICĂ 14

4.1. DIAGRAMELE ELLINGHAM 14

4.2. CALCULELE ABATERILOR 17

4.2.1. CALCULAREA ABATERILOR PENTRU GRAFIT/TIC 17

4.2.2. CALCULAREA ABATERILOR PENTRU GRAFIT/TIN 17

4.2.3. CALCULAREA ABATERII PENTRU NITRURILE DE GRAFIT/(MG-SI-AL) 18

5. METODOLOGIA DE CERCETARE 20

5.1. STRATEGIA EXPERIMENTALĂ 20

5.2. REZULTATE EXPERIMENTALE. GRAFIT LAMELAR 21

5.2.1. INFLUENȚA ADĂUGĂRII DE SULF 26

5.2.2. INFLUENȚA ADAOSULUI DE TITAN 27

5.2.3. INFLUENȚA NUCLEELOR ASUPRA CREȘTERII GRAFITULUI 27

5.3. REZULTATE EXPERIMENTALE. GRAFIT „TADPOLE“ 28

5.4. REZULTATE EXPERIMENTALE. GRAFIT COMPACTIZAT 31

5.4.1. EFECTUL ADAOSULUI DE TITAN ÎN METALUL DE BAZĂ 35

5.4.2. EFECTUL PROCESULUI DE INOCULARE 38

5.4.2.1. INOCULANTUL Ce 38

5.4.2.2. INOCULANTUL ZrMn 39

5.4.3. EFECTUL TIMPULUI DE RĂCIRE RAPIDĂ 39

5.4.4. INFLUENȚA NUCLEELOR ÎN CREȘTEREA GRAFITULUI 40

5.5. REZULTATE EXPERIMENTALE. GRAFIT SFEROIDAL 41

5.5.1. EFECTUL ADAOSULUI DE TITAN ÎN METALUL DE BAZĂ 44

5.5.2. EFECTUL PROCESULUI DE INOCULARE 49

5.5.2.1. INOCULANTUL Ti 50

5.5.2.2. INOCULANTUL Ba 50

5.5.2.3. INOCULANTUL Ce 50

5.5.2.4. INOCULANTUL ZrMn 51

5.5.3. EFECTUL TIMPULUI DE RĂCIRE RAPIDĂ 51

5.5.4. INFLUENȚA NUCLEELOR ÎN CREȘTEREA GRAFITULUI 52

6. CONCLUZII FINALE 54

7. CONTRIBUȚII ORIGINALE ȘI DIRECȚII DE CERCETARE VIITOARE 56

8. BIBLIOGRAFIE 58

1. INTRODUCTION

Cast iron is a group of iron-carbon alloys with a carbon content greater than 2% [1], whose history goes back more than 1.600 years. Carbon ranging from 1.8-4wt%, and silicon 1-3wt% are the main alloying elements of cast iron, being iron alloys with lower carbon content (≈0.8%wt) known as steel. While this technically makes the Fe-C-Si system ternary, the principle of cast iron solidification can be understood from the simpler binary iron-carbon phase diagram, which can be stable (Fe graphite) or metastable (Fe-Fe_3C) depending on a series of factors, such as, chemical composition, cooling rate or the number of nucleation sites. The most recent diagram is shown in Figure 1 [2].

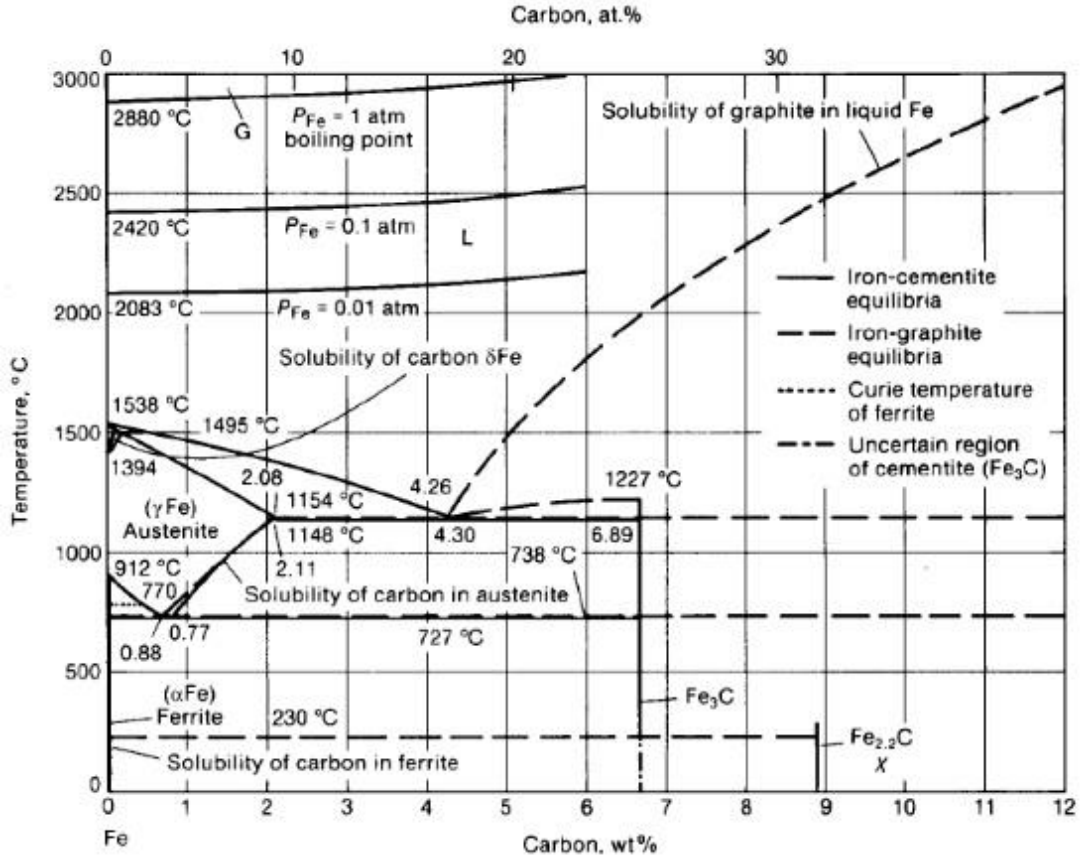

Figure 1. Fe-C stable and metastable diagram.

Cast iron is known as hypoeutectic when the primary phase to precipitate is the austenite and hypereutectic when the primary phase is the graphite. Based on the graphite structure, several types of cast iron can be identified: gray cast iron, compacted graphite cast iron, ductile cast iron, white cast iron and malleable cast iron (Figure 2). From all of them, gray iron (with flake graphite) and ductile iron (with spheroidal graphite) can be considered as the two main types.

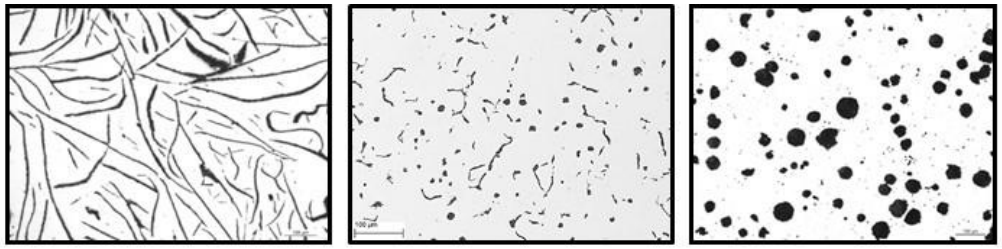

Figure 2. Types of cast iron.

Gray Cast Iron (LGI)

It is also known as lamellar graphite iron and it is characterized by its graphitic microstructure, which causes fractures of the material to have a grey appearance. It is the most commonly used cast iron and the most widely used cast material based on weight. Most cast irons have a chemical composition of 2.5–4.0% carbon, 1–3% silicon. In two dimensions, the graphite flakes appear as fine lines with different distributions and sizes and are interconnected with the eutectic grain, classifying the graphite in five categories according by the ASTM standard A-247: type A, B, C, D and E (Figure 3).

Figure 3. Types of lamellar (flake) graphite (FG).

Ductile Cast Iron (DI or SGI)

Ductile iron, also known as nodular cast iron or spheroidal graphite iron, is not a single material but part of a group of materials which can be produced with a wide range of properties through control of their microstructure. The common defining characteristic of this group of materials is the shape of graphite which is in the form of nodules or spheroids. Nodule formation is achieved by adding nodulizing elements, most commonly magnesium (0.04%Mg) and less often now, cerium.

Compacted Graphite Cast Iron (CGI)

This type of cast iron also known as vermicular graphite iron is characterized by a worm-like shape graphite, rounded and interconnected between them and within the eutectic cell similar to lamellar graphite in gray iron. Both the microstructure and the properties can be considered roughly intermediate between gray and ductile iron [3,4,5]. The CGI is produced through liquid treatment similar to that of SGI, but with lower magnesium content (0.02%Mg).

2. FUNDAMENTALS OF SOLIDIFICATION OF CAST IRON

Solidification is the result of the formation of stable clusters of long-range order atoms in the liquid (nucleation), followed by their growth. The classic nucleation theory assumes that these clusters of atoms or molecules from spontaneously in the matter undergoing transformation, resulting in a constant nucleation rate. This nucleation is directly related to the widely used inoculation processes of cast iron, which is used to control the grain and graphite size and, to a lesser extent, graphite morphology.

2.1. PROCESS OF NUCLEATION

It is postulated that even in the absence of carbon addition to the melt, graphite can nucleate on carbon rich regions in the melt. Below the equilibrium transformation temperature, fluctuations in density, atomic configurations, heat content, etc., occur in the liquid. They make possible the formation of minute particles of crystalline solid (long-range order) called **embryos**. As a result, the free energy of the system increases, and, unless enough undercooling is available, the embryo will remelt. If the undercooling of the melt is sufficient, the embryo will survive, and will grow to form a **nucleus**. This type of nucleation is known as **homogeneous nucleation**.

The undercooling required for homogeneous nucleation is rather high. In fact, this type of nucleation is the most difficult kinetic path for crystal formation. According to the Hollomon and Turnbull theory (1953)[6], homogeneous nucleation is only possible for supercooling in the order of $0.25T_f$, and undercoolings of this magnitude have never been observed in commercial casting alloys, since the order of magnitude of the undercooling is only a few tens of degrees, at maximum. However small contamination particles in the melt by additions of chemicals made on purpose (called grain refiners or inoculants), oxides on the melt surface or contact with the walls of a mold, may catalyze nucleation at a much smaller supercooling and with fewer atoms required to form the critical nucleus. This nucleation occurring on solid substrates foreign to the metal, is called **heterogeneous nucleation**.

2.1.1. CONDITIONS FOR GRAPHITE CRYSTALLIZATION

The development of any solid crystal or crystallite from the liquid phase is initiated by a nucleus. The heterogeneous nucleation theory developed during the last decades is focused on non-metallic inclusions, which must satisfy some specific conditions to act as possible nucleation sites:

- The substrate must be solid in the melt; its melting point must be higher than the melt temperature, and it must not dissolve in the melt
- Low contact angle between metal and nucleant particles or high surface energy between the liquid and the nucleant , γ_{nL}; indeed if $\gamma_{nL} > \gamma_{nS} + \gamma_{LS}\cos\theta$, the nucleus can spread on the substrate and grow; on the other hand, if $\gamma_{nL} < \gamma_{nS} + \gamma_{LS}\cos\theta$, the nucleus must shrink and disappear

- The nucleant must expose a large area to the liquid what can be achieved producing a fine dispersion of nucleant, or by using a nucleant with a rough surface geometry
- Because the atoms are attaching to the solid lattice of the substrate, the closer the substrate lattice resembles that of the solid phase, the easier nucleation will be. This means that, ideally, the crystal structure of the substrate and the solid phase should be the same. As the crystal structures of the solidifying alloy and the substrate may be different, the substrate must have one or more planes with atomic spacing and distribution close to that of one of the planes of the solid to be nucleated (coherent or semi-coherent interface), i.e, have a low linear disregistry δ [7]:

$$\delta = (\boldsymbol{a_n} - \boldsymbol{a_S})/\boldsymbol{a_S} \qquad \textbf{Equation 1}$$

  where a_S and a_n, are the interatomic spacing along shared low-index crystal directions in the solid nucleus and the nucleant, respectively
- Low symmetry lattice (complex lattice): while it is impossible to assign numbers to lattice symmetry, to some extent the entropy of fusion can be used as a measure of lattice symmetry. In general, less symmetrical lattices have higher entropies of fusion
- Ability to nucleate at very low undercooling

From all requirements which should satisfy an efficient heterogeneous nucleant, most of investigators have tried to relate directly heterogeneous nucleation behavior to crystallographic disregistry, probably due to the possibility to quantify it.

According to the theory advanced by Turnbull and Vonnegut [7], a nucleating agent will be effective in promoting nucleation when the lattice parameters in the low-index crystallographic planes of both the substrate and the nucleated solid are similar. However, Bramfitt (1970) [8] concluded that this equation for linear disregistry (Equation 1) places a strict limitation on the selection of a crystallographic relationship, because the equation is restricted to the choice of planes of similar atomic packing for the substrate and nucleated solid. Therefore, in order to broaden their equation so that it would be applicable to crystallographic combinations of two phases with planes of differing atomic arrangements, it was found necessary to modify the equation in terms of angular difference between the crystallographic directions with the planes.

These planar disregistry equation can be presented in two different forms, the first of which is the generalized one:

$$\boldsymbol{\delta} = \frac{\boldsymbol{\delta_1}+\boldsymbol{\delta_2}+\boldsymbol{\delta_3}}{\mathbf{3}}\boldsymbol{x100} \qquad \textbf{Equation 2}$$

where δ_1, δ_2 and δ_3 are the disregistries calculated along the three lowest-index directions within a 90 deg quadrant of the planes of the nucleated solid and the substrate. The second, or more specific, form of the modified equation is as follows:

$$\delta_{(hkl)_n}^{(hkl)_s} = \sum_{i=1}^{3} \frac{\frac{\left|\left(d_{(uvw)_s^i} \cos\theta\right) - d_{(uvw)_n^i}\right|}{d_{(uvw)_n^i}}}{3} x100 \qquad \textbf{Equation 3}$$

where $(hkl)_s$ is a low-index plane of the substrate, $[uvw]_s$ is a low-index direction in $(hkl)_s$, $(hkl)_n$ is a low-index plane in the nucleated solid, $[uvw]_n$ is a low-index direction in $(hkl)_n$, $d_{[uvw]_n}$, is the interatomic spacing along $[uvw]_n$, $d_{[uvw]_s}$ is the interatomic spacing along $[uvw]_s$ and θ is the angle between $[uvw]_s$ and the $[uvw]_n$.

This last equation gives the same results for cubic systems as Equation 24, but significantly different for hexagonal systems.

Table 1. Nucleating agents for pure iron.

NUCLEANT	CRYSTAL STRUCTURE	LINEAR DISREGISTRY	PLANAR DISREGISTRY	UNDERCOOLING (ºC)	EFECTIVENESS
none	cubic	x	x	30-55	x
TiN	cubic	3.9	3.9	1.7	high
TiC	cubic	5.9	5.9	1.8	high
SiC	cubic	6.0	6.0	x	moderate
ZrN	cubic	11.2	11.2	7.0	moderate
ZrC	cubic	14.4	14.4	13.6	low
WC	hexagonal	29.4	12.7	16.1	low

As it can be seen from the disregistry data in Table 1, when the planar disregistry is less than about 12 pct, the nucleating agent is potent; whereas the disregistry is above 12 pct, the potency is poor, which is in close agreement with the Reynolds and Tottle theory [9]. It must be noted, that for cubic metals there was no difference between the linear and planar disregistry, but for hexagonal WC the planar disregistry was much lower than the linear one.

2.2. NUCLEATION OF GRAPHITE

The heterogeneous nucleation theory developed over the last 30 years is based on non-metallic inclusions present in all commercial cast irons, such as oxides, nitrides, sulfides and silicates which can act as possible nucleation sites when verify the specific conditions previously described. The three main types of graphite (lamellar, compacted and spheroidal) nucleate in these types of substrates, although the chemistry of them is different in any case.

A multitude of theories have been proposed with the objective to explain the nucleation process of spheroidal and lamellar graphite (SG and LG respectively). Nevertheless, the mechanism has still not been totally clarified, due to the composition of the nuclei is highly variable (mainly due to the highly non-equilibrium conditions under which they are formed), the high temperatures and the complex reactions which occur during the solidification of cast iron. All these causes make difficult to obtain a clear and simple answer of the nucleation process. In the case of compacted graphite (CG), its complex 3D morphology has hindered significant advances in similar theories for this type of graphite and there is hardly any information about it in the literature.

2.2.1. NUCLEATION OF LAMELLAR GRAPHITE

Nucleation of LG can occur on carbon-rich regions in the liquid, such as carbon molecules or undissolved graphite. These carbon-rich clusters may serve as homogeneous nuclei for the graphite [10,11]. Another example of the one-stage nucleation model is the salt-like carbides nucleation theory advanced by Lux [12], based on experiments that found that pure metals such as lithium, calcium, barium, strontium and sodium [13] promote graphite nucleation in LG iron. Lux suggested that all elements from groups I, II, and III from the periodic table, when are introduced in molten iron, form salt-like carbides that develop epitaxial planes with the graphite acting as nuclei. Other carbides, such as TiC or Ti(CN), have been demonstrated to act as nuclei for LG [14], although in a rather limited manner.

The first multi-stage nucleation mechanism was proposed by Weiss, who argued that nucleation of LG occurs on SiO_2 oxides formed by heterogeneous catalysis on CaO, Al_2O_3 and oxides of other alkaline metals [15]. Later, Wallace [16] revealed the role of MnS or complex (MnX)S in graphite nucleation as a consequence of their low crystallographic misfit with the graphite [17,18]. Sommerfeld and Ton [19] found that manganese sulfides contained additional elements such as Al or Mg when small amounts of Mg were added to the melt. The (MnMg)S particles had the same shape, color and distribution as the MnS particles. Riposan et al [20]proposed that graphite nucleation starts with the precipitation of complex oxides of Al, Si, Zr, Mg, Ti followed by the growth of complex (MnX)S sulfides, which constitute the nuclei for flake graphite.

2.2.2. NUCLEATION OF COMPACTED GRAPHITE

While the manufacture of CGI castings has seen significant expansion over the recent years, the nucleation of CG during iron solidification is still not fully understood. Compacted graphite is only stable at low levels of oxygen and sulfur, since magnesium is a very strong sulfide former, magnesium sulfide (MgS) inclusions are formed preferentially to manganese sulfide (MnS). These MgS inclusions have been identified previously as good nuclei for compacted graphite [21].

Titanium is typically present in cast irons in the range of 0.005-0.02% Ti. The compatibility between titanium with carbon and/or nitrogen present in the molten iron promotes the formation of titanium carbonitride inclusions, which form in the liquid state and grow with a cubic shape. Yet Sun and Loper

[22] found titanium carbonitride particles embedded in compacted graphite and hinted to the possibility of Ti(CN) acting as weak nucleant.

2.2.3. NUCLEATION OF SPHERODIAL GRAPHITE

Nucleation of SG is even more complex than that of LG and there are many theories which have tried to explain this phenomenon in solidifying cast iron. As it happened with the lamellar graphite, all the theories postulated in the category of homogeneous nucleation can be applied to spheroidal graphite and it is in the study of heterogeneous nucleation (one or multi-stage nucleation) where appear the main differences.

Some of these theories are based on formation of SG on gas bubbles produced by the evaporation of Mg [23,24,25], or on salt-like carbides with cubic structure formed by elements from groups I (Na, K), II (Mg, Ca, Sr, Ba) and III (Y, La) from the periodic table [14]. This last theory would not be supported by thermodynamics, due to according to data exposed in Table 2, the free energy of formation of carbides of these elements is at least two-three times higher than that of their sulfides or oxides.

Table 2. Melting points and standard free energy (in J/mol) of formation of selected sulfides, carbides, nitrides, oxides and silicates: a) Ref. [23] (at ΔG at 1327ºC); b) https://en.wikipedia.org/wiki/wiki; all other Factsage (ΔG at 1200ºC).

Compound	Melting Temp., (ºC)	ΔG (J/mol)	Compound	Melting Temp., (ºC)	ΔG (J/mol)	Compound	Melting Temp., (ºC)	ΔG (J/mol)
Complex oxides			***Oxides***			***Nitrides***		
$2MgO\ 2CaO\ 14Al_2O_3$		-2.62E+07	Al_2O_3	2072[b]	-1.21E+06	ZrN	2952[b]	-6.10E+05
$3CaO\ Al_2O_3\ 3SiO_2$		-4.85E+06	Fe_3O_4		-6.49E+05	TiN	2930[b]	-5.80E+05
$2MgO\ CaO\ 2SiO_2$		-3.98E+06	SiO_2		-6.49E+05	AlN	2200[b]	-5.38E+05
$2CaO\ FeO\ SiO_2$		-3.70E+06	MgO	2832[a]	-5.85E+05	CeN		-5.32E+05
$5CaO\ 4TiO_2$		-5.47E+06	CaO	2927[a]	-4.78E+05	Ca_3N_2		-1.39E+05
			Ti_2O_3		-1.12E+06	Mg_3N_2	1500[b]	-1.18E+05
Double oxides			***Sulfides***			***Carbides***		
$3CaO\ 2SiO_2$		-2.96E+06	CaS	2450[a]	-4.25E+05	TiC		-1.63E+05
$2MgO\ SiO_2$	1898[a]	-1.57E+06	MgS	2000[b]	-2.94E+05	Al_4C_3		-1.23E+05
$Al_2O_3\ SiO_2$		-1.86E+06	CeS		-4.07E+05			
$SrO\ SiO_2$	1580[a]	-1.19E+06	SrS	2000[a]	-3.70E+05			
$BaO\ SiO_2$	1605[a]	-1.18E+06	BaS	2227[a]	-3.56E+05	***Carbo-nitrides***		
$MgO\ SiO_2$	1577[a]	-1.11E+06	Ti_2S_3		-6.38E+05	$CaCN_2$		-1.39E+05
$2FeO\ SiO_2$		-1.01E+06	ZrS_3		-5.11E+05			
$5CaO\ 4TiO_2$		-5.47E+06						

Other theories are focused on a dual structure of nuclei in SG, with a core made of Ca-Mg sulfide for the Mg-treated iron surrounded by an outer shell of Mg-Al-Si-Ti oxide [21].These findings led to the two-stage theory of nucleation of SG in cast iron, which proposes that initial sulfides serve as catalytic substrates for oxides, on which the spheroidal graphite nucleates. Although perhaps the most elaborate

theory was advanced by Skaland et al. [23] who argued that the majority of the inclusions in ductile iron are primary or secondary products of the Mg treatment, and reported that the hexagonal nuclei are composed of double layer compounds, namely a sulfide (MgS and CaS) core surrounded by silicates (MgO SiO_2 and 2 MgO SiO_2) on which epitaxial graphite growth occurs.

2.3. GROWTH OF GRAPHITE

Graphite is one of the two naturally occurring forms of crystalline carbon. The other natural allotrope is diamond. Above 900 C the diamond structure is transformed into graphite. While diamond has a face-centered cubic lattice, graphite has a layer-structure of graphene layers in which the carbon atoms are arranged in a honeycomb lattice with separation of 0.142 nm, and the distance between planes of 0.335 nm. The strong sigma-bonds in layers and weak Pi-bonds between layers produce the faceted morphology and high anisotropic behavior of graphite. As suggested by the Bravais's rule and the Gibbs-Wulff theorem, typically graphite grows faster along the tightly-bond *a*-axis directions [1010], rather than the loosely-bond *c*-axis direction [0001].

Graphite morphology is the result of crystallization controlled by attachment kinetics, followed by solid diffusion growth. The chemical complexity of the iron melts, and the transitory nature of nucleation, local segregation and cooling rate, are the reasons for the large variety of graphite morphologies found in industrial cast irons. They include the “standard” shapes: lamellar/flake (LG), compacted/vermicular (CG), spheroidal/nodular (SG), and temper graphite (in malleable iron). In addition, some “degenerated” morphology, such as spiky, exploded, or chunky graphite, can result from incorrect melt treatment or unfavorable cooling conditions [24]. Some typical examples of graphite shapes, illustrating the complex morphology are presented in Figure 4 [25,26,27,28].

Interrupted solidification experiments revealed that the basic building blocks of the graphite aggregates are hexagonal faceted graphite platelets with nanometer height in the c-direction and micrometer width in the a-direction.

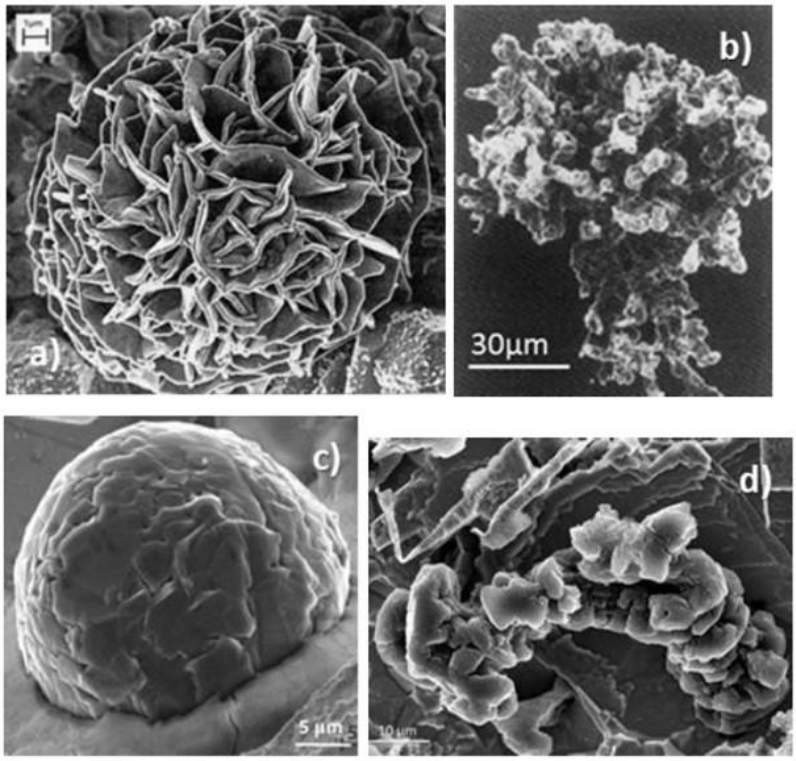

Figure 4. Typical graphite shapes found in commercial cast iron: a) LG aggregates; deep etching [5]; b) extracted CG aggregate [26]; c) SG; deep etching [27]; d) chunky graphite; deep etching [28].

2.3.1. SOLIDIFICATION OF LAMELLAR GRAPHITE (LG)

Dendritic branching in lamellar graphite has been described by Lux et al. [29], where the eutectic crystals of graphite branch out of lamellar edges. The branches bend and overlap the original graphite plate.

The SEM analysis of deep-etched interrupted solidification hypoeutectic samples shows that in the initial stage lamellar graphite grows from the liquid, at the γ/L interface, as crystalline hexagonal parallel platelets, with growth morphology consistent with that of foliated dendrites. The platelets then may stack into curved plates (lamellae) that grow radially from a common center.

2.3.2. SOLIDIFICATION OF COMPACTED GRAPHITE (CG)

Some investigations [30,31] have demonstrated that CG is interconnected to their nearest neighbours within the eutectic grain quite similar to lamellar graphite, which makes it difficult to locate their nucleation sites. Using polarized light, it has been suggested that a similar crystallographic orientation occurs in SG and in the segmented features of CG [32].

Pan et al [33] performed interrupted solidification experiments on thermal analysis cups to study the solidification of CG irons, obtaining qualitative information on graphite shape evolution. The authors

concluded that initial graphite precipitates in a spherical shape, which degenerates early during subsequent solidification, and then develops into CG. Similar conclusions were obtained by Alonso et al. [34]. These researchers claimed that the SG-to-CG transition occurred when the spheroidal graphite developed a tail (tadpole graphite). In the regions where the SG started generating tails that become CG, branching of graphite appears to occur through twin boundaries defects that result in the splitting of the lamellae along the basal plane.

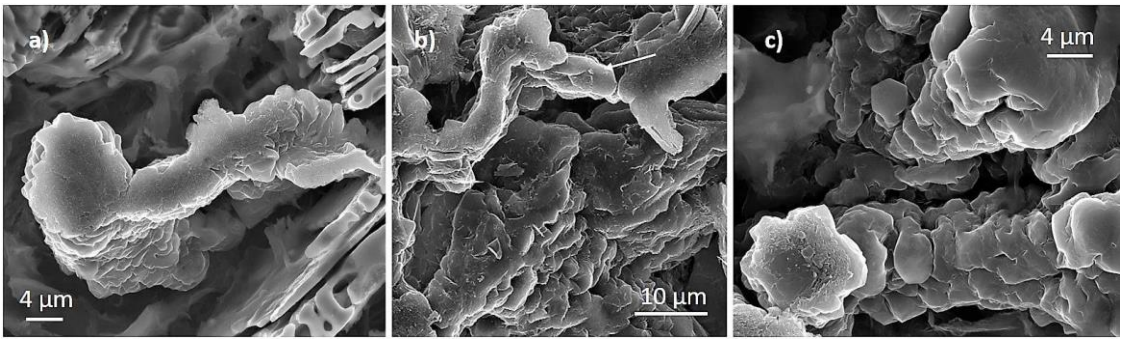

Figure 5. Stacking of graphite plates along the c-direction to produce various forms of graphite: a) tadpole graphite; b) compacted graphite; c) chunky graphite [28].

Additions of Mg or Ce increasingly change the crystallization pattern of graphite with the addition level. SEM analysis of interrupted solidification experiments of low-magnesium iron (0.013-0.02% Mg) reveals a gradual change from stacking of platelets along the *a*-direction in the tiled-roof configuration, to stacking in the *c*-direction. Figure 5a exhibit a tadpole graphite constructed of *c*-direction stacked platelets. Further branching of the graphite dendrite will produce compacted graphite (Figure 5b). Stacking of the platelets in columnar structures, as in Figure 5c, may produce graphite similar to chunky graphite. The hexagonal shape of the platelets is less regular, indicating a roughening of the interface produced by the higher constitutional undercooling induced by Mg.

2.3.3. SOLIDIFICATION OF SPHEROIDAL GRAPHITE (SG)

The room temperature graphite spheroid is the product of three processes (Figure 6)[35]: i) nucleation and growth in the liquid; ii) growth during the eutectic transformation via carbon diffusion through the austenite shell; iii) growth during cooling to room temperature as the solubility of carbon in austenite decreases. Stage I produces spherical aggregates. During stage II graphite grows through conical sectors that appear to nucleate on the spheroids produced in stage I. For a well-formed spheroid, the sectors grow in contact with one another. The separated graphite conical sectors in Figure 6b indicate the beginning of formation of degenerated graphite. In this case, growth of the platelets in the *a*-direction is

inhibited and the sectors do not contact one another, entrapping austenite between them. Sometimes, the graphite nodule may exhibit the nucleus and all three stages, as seen in Figure 6c.

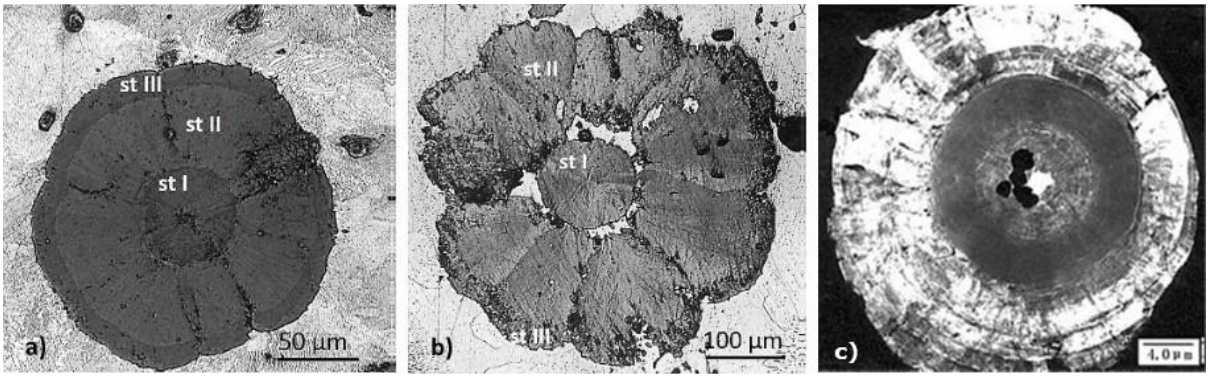

Figure 6. Three-stage growth of a graphite spheroid: a) optical image of well-formed graphite spheroid (compliments of J. Barlow and A. Catalina, Caterpillar Inc.); b) optical micrograph of a degenerated (exploded) graphite spheroid (complements of A. Udroiu) [123]; c) in an as-cast microstructure; TEM image [36].

A proliferation of papers using Transmission Electron Microscopy to analyze and interpret the room temperature microstructure of spheroidal graphite has occurred in recent years. The pioneering TEM work of Purdy and Audier [37] demonstrated that after encapsulation of the graphite spheroid into an austenitic shell, graphite growth continues through solid diffusion of carbon through the austenite to the growth front. The amorphous carbon deposited at the graphite/austenite interface crystallizes to produce graphite platelets.

TEM work by Hara et al. [38] shows a three-fold internal structure for SG, with and amorphous central region, annular rings of a layered intermediate region, and an outer region made of large polygonal crystalline platelets in a mosaic-like structure. It appears that no sulfide, oxide or nitride core was necessary for the formation of graphite spheroids.

3. OBJECTIVES

As it has been demonstrated in the extensive literature review of the previous section, there are many researchers who have tried to explain the phenomena of nucleation and growth of graphite during the last 50-60 years, developing tens of theories that with more or less reliability have given a response to these complex processes.

The main objective of this thesis is to provide some clarity to the phenomena of nucleation in the three main types of graphite, lamellar (LG), compacted (CG) and spheroidal (SG), complementing the conclusions already obtained by other authors or even developing other theories.

The final goal is complex, ambitious and very complicated to approach it directly, so the idea is to divide it in other ones simpler, which allow to obtain a truthful information. Some of these objectives are:

- To develop some theoretical calculations (Ellingham's diagrams and disregistry parameters) which complement the information already available on this topic
- To reveal experimentally, the main inclusions which can appear in spheroidal, compacted and lamellar graphite
- To identify the nature of nucleation sites for the three main type of graphite (LG, CG and SG), through the use of Advanced Field Emission Gun Scanning Electron Microscope (FEG-SEM) techniques
- To attempt further understanding of the role of some elements present in the base iron (as titanium and sulfur) in the nucleation of graphite
- To understand the effect of the inoculation in the nucleation process
- To analyze the influence of some trace elements (Ca, Al, Zr, Ba, La, Ce) in the type of non-metallic inclusions (sulphides, oxides, carbides, nitrides and silicates) which can act as nuclei for graphite
- To study the impact of the nucleation sites in the growth of graphite

4. THEORETICAL CONTRIBUTION

4.1. ELLINGHAM'S DIAGRAMS

An Ellingham diagram, is a graph showing the temperature dependence of the stability for compounds. In the case of nucleation of graphite, these compounds are mainly, oxides, sulfides and nitrides that can act as nucleation sites if they verify certain requirements, including a high stability which is defined by a low standard free energy of formation.

There is not too much information in the literature about the reactions of a metal with sulfur, nitrogen and other non-metals. With the objective to add some contribution to this field and with the use of the thermochemicalc software, F*actsage*, two Ellingham's diagrams, one for sulfides (Figure 7) and another one for nitrides (Figure 8) have been built. These diagrams will give enough information to study the comparative stability of different compounds across a range of partial pressures and temperatures

All the reactions are normalized to consume one mole of S2 (for sulfides) and N2 (for nitrides) (similar to oxides) and in both cases, reactions closer to the top of the diagram are the most "noble" metals, and their sulfides and nitrides are unstable and easily reduced. On the other side, the lower the position of a metal's line in the Ellingham diagram, the greater is the stability of its sulfide and nitride. In the Ellingham's diagram for sulfides, P sulfides would be the least stable (they have never found acting as nuclei) versus Ca sulfide as most stable sulfide. In the case of nitrides, MgN from 1100ºC and MnN are the least stable versus TiN (a typical nucleation site). The greater the gap between any two lines, the greater the effectiveness of the reducing agent corresponding to the lower line.

Most of the curves in the Ellingham diagrams for the formation of sulfides and nitrides (with the exception of ZrS) are basically straight lines with a positive slope, decreasing their stability with increase in temperature. Mg, Ca, and RE sulfides and Ti, Al nitrides, present the lowest values of standard free energy of formation, what would become in the most suitable nucleation sites for graphite from thermodynamic point of view. In the case of nitrides, the number of compounds is very limited, because most of them were unstable and presented positive values of energy of formation.

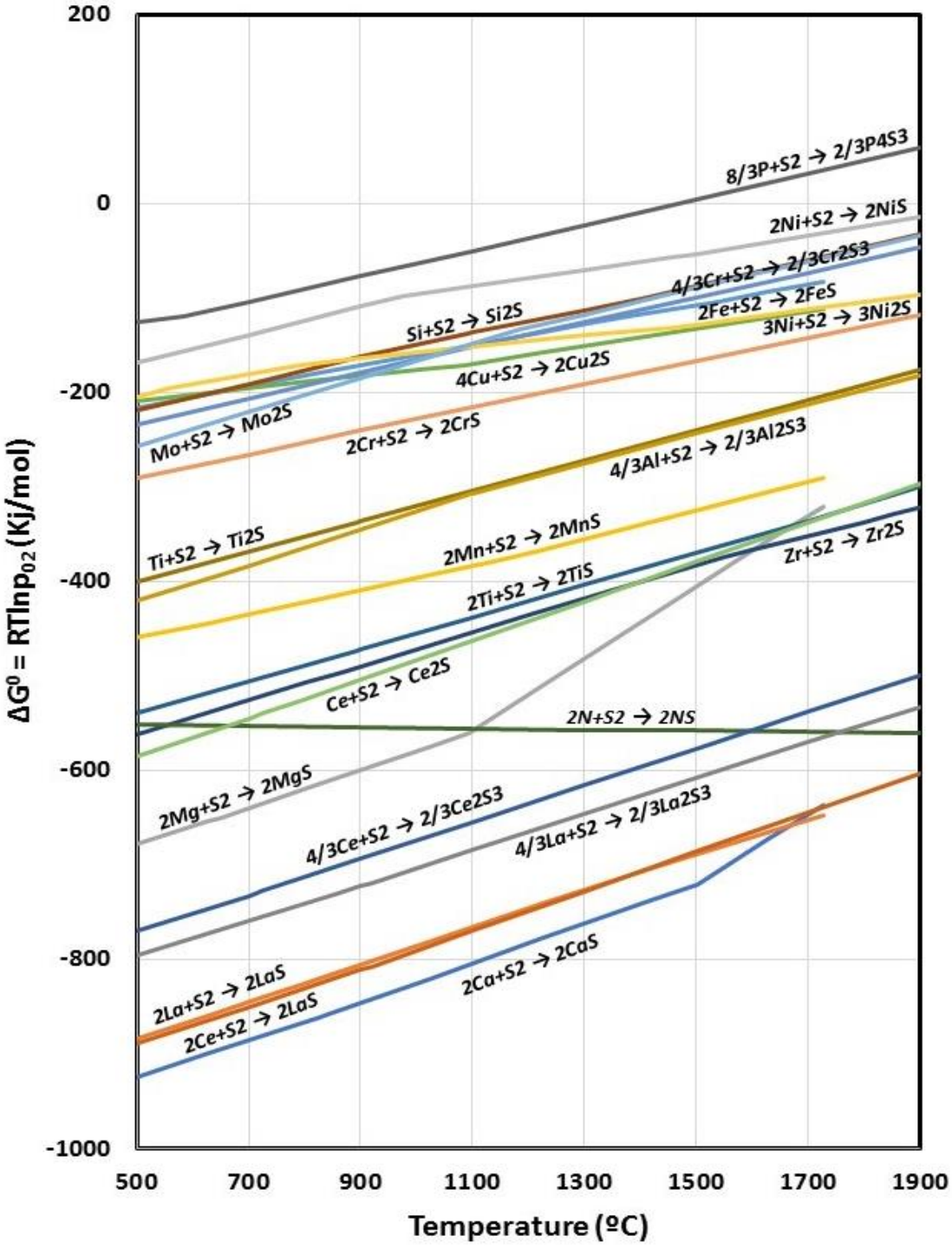

Figure 7. Standard free energy of formation of some selected sulfides, corresponding to the general reaction (2x/y)M + S2=(2/y)MxSy.

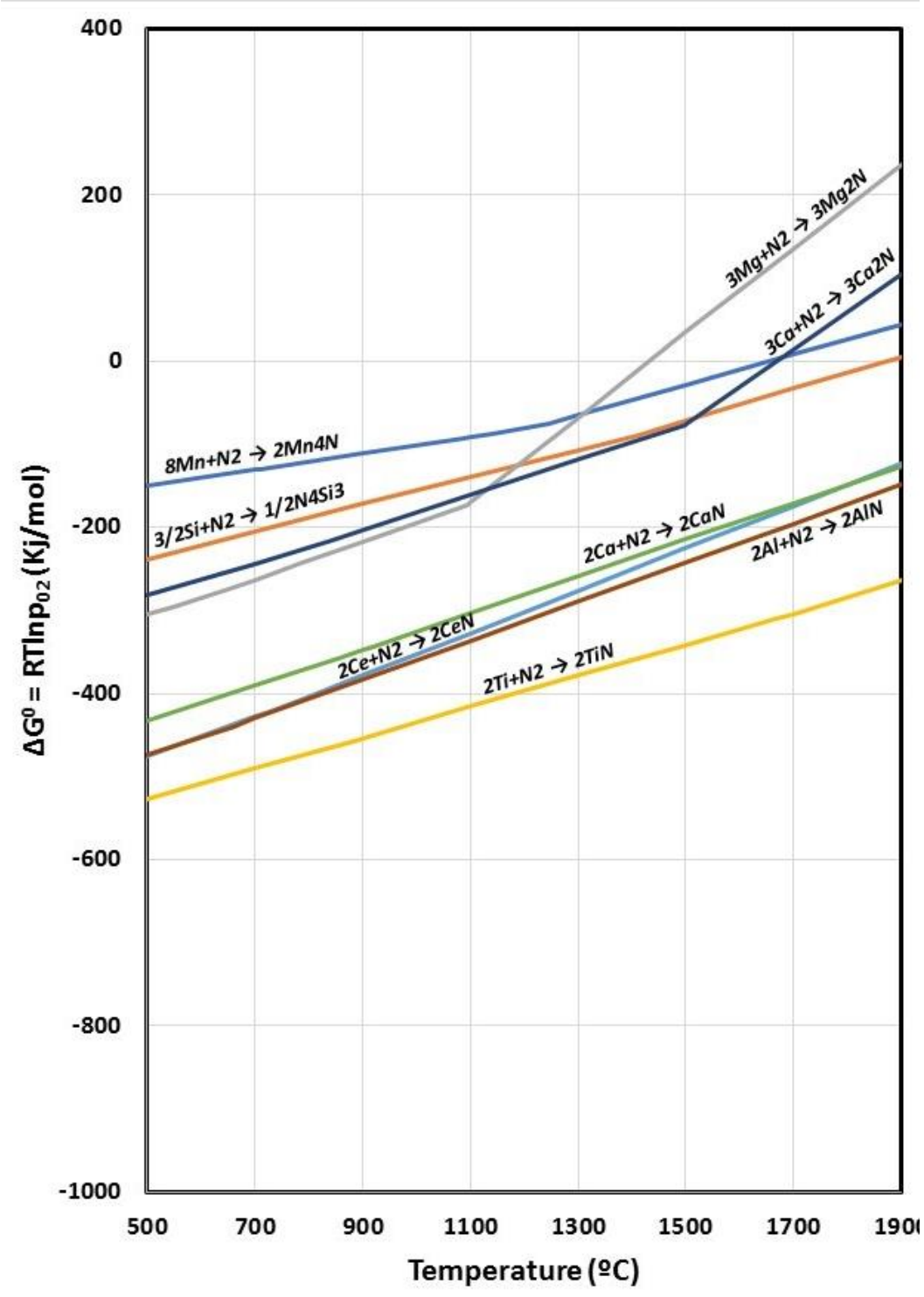

Figure 8. Standard free energy of formation of some selected nitrides, corresponding to the general reaction (2x/y)M + N2=(2/y)MxNy.

4.2. DISREGISTRY CALCULATIONS

An efficient heterogeneous nucleant requires a coherent or semi-coherent interface between the nucleating substrate and the growing solid. This condition can be calculated from the disregistry parameter (Equation 3), which is a measure of the difference between the lattice parameter of the two materials. There is little evidence of the quantification of this parameter for inclusions as carbides or nitrides which play also an important role in the nucleation process. In this thesis, it is going to try to solve this lack of information.

4.2.1. CALCULATION OF GRAPHITE/TiC DISREGISTRY

The propensity of TiC of serving as a nucleant for graphite was discussed by Sun and Loper [14] from the standpoint of linear disregistry. They argued that while the atomic structure of TiC is such as to act as nucleus for graphite, the degree of mismatch between the lattices would minimize its nucleation effectiveness. As discussed previously, the Turnbull/Vonnegut equation for linear disregistry cannot be applied to crystallographic combinations of two phases with planes of differing atomic arrangements, such as cubic Ti(CN) and hexagonal graphite. Consequently, planar disregistry calculations must be performed.

TiC has a cubic crystal structure with a lattice parameter a=0.4327 nm. Position coordinates of the atoms form the (010) plane for TiC crystals, and directions and interatomic distances of carbon atoms along the direction in this cell are summarized in Table 3.

Table 3. Parameters for the calculation of graphite/TiC planar disregistry.

No.	Case	$[hkl]_{TiC}$	$[hkl]_{G}$	$d_{[hkl]TiC}$	$d_{[hkl]G}$	α, deg	$d_{[hkl]TiC}$
1	$(\bar{1}012)_G \| \|(010)_{TiC}$	[100]	[0100]	0.4327	0.426	0	0.4327
2		[101]	$[\bar{1}311]$	0.6119	0.5954	40’50’’	0.6118
3		[001]	$[\bar{1}011]$	0.4327	0.416	0	0.4327

Using the data from Table 3 in Equation 3, it was calculate that $\delta_{G/TiC} = 2.69\%$ what suggests the possibility of formation of a layer of carbon atoms on the surface of TiC.

4.2.2. CALCULATION OF GRAPHITE/TiN DISREGISTRY

In addition to form TiC, titanium can combine with the nitrogen forming TiN, which has a cubic crystal structure with a lattice parameter a=0.4256 nm. Calculations are similar to TiC and the data are summarized in

Table 4. Using these data in equation 3, it was found that $\delta_{G/TiN} = 1.11\%$.

As for the graphite/TiC calculations, the small order disregistry suggests the possibility of formation of a layer of carbon atoms on the surface of the TiN, with ordering specific to the cell for which the disregistry was calculated.

Table 4. Parameters for the calculation of graphite/TiN planar disregistry.

No.	Case	$[hkl]_{TiN}$	$[hkl]_G$	$d_{[hkl]TiN}$	$d_{[hkl]G}$	α, deg	$d_{[hkl]TiN}$
1	$(\bar{1}012)_G \| \|(010)_{TiN}$	[100]	[0100]	0.4256	0.426	0	0.4256
2		[101]	$[\bar{1}311]$	0.6019	0.5954	40'50''	0.6013
3		[001]	$[\bar{1}011]$	0.4256	0.416	0	0.4256

4.2.3. CALCULATION OF GRAPHITE/(Mg-Si-Al) NITRIDES DISREGISTRY

While disregistry calculation of the complex (MgSiAl)N is not possible because of the absence of necessary data on its crystallographic structure, calculation will be performed for the magnesium and aluminium nitrides. All data are summarized in Table 5.

Table 5. Data for calculation of planar disregistry graphite-Mg_3N_2.

No.	Planar disregistry between	$[uvw]_{Mg3N2}$	$[uvw]_G$	$d^{Mg3N2}_{[uvw]}$	$d^{G}_{[uvw]}$	α, deg	$d^{Mg3N2}_{[uvw]} \cdot cos\alpha$	δ, %
1	P_0 and Mg_3N_2	[100]	[0100]	0.995	0.994	0	0.995	$\delta_0 = 0.59$
2		[101]	$[\bar{4}740]$	1.407	1.399	17'23'	1.4068	
3		[001]	$[\bar{4}040]$	0.995	0.984	0	0.995	
4	P_1 and Mg_3N_2	[100]	[0100]	0.995	0.852	0	0.995	$\delta_1 = 6.47$
5		[101]	$[\bar{4}641]$	1.407	1.344	5°40'2	1.337	
6		[001]	$[\bar{4}041]$	0.995	0.1040	0	0.995	
7	P_2 and Mg_3N_2	[100]	[0100]	0.995	0.994	0	0.995	δ_2
8		[101]	$[\bar{3}732$	1.407	1.408	5'52''	1.407	
9		[001]	$[\bar{3}032$	0.995	0.997	0	0.995	
10	P_3 and Mg_3N_2	[100]	[0100]	0.995	0.852	0	0.995	$\delta_3 = 7.57$
11		[101]	$[\bar{1}613$	1.407	1.341	5°34'1	1.400	
12		[001]	$[\bar{1}013$	0.995	0.1036	0	0.995	

The small values of these parameters, and in particular δ_0 and δ_2, suggest near perfect coherency and hence the possibility of graphite nucleation on Mg_3N_2. The most favourable are the plane P_0 and P_2, in which cells with dimensions almost identical with the unit cell of Mg_3N_2. were found.

A similar analysis was conducted for AlN, which has a hexagonal lattice with the parameters *a* = 0.311 nm and *b* = 0.498 nm [39]. Using the Equation 3 and the data presented in

Table 6, it was found a disregistry $\delta_4 = 7.586\%$, which implies that graphite can grow on the prism faces of AlN.

Table 6. Data for calculation of planar disregistry graphite-AlN.

No.	Planar disregistry	$[uvw]_{AlN}$	$[uvw]_G$	$d^{AlN}_{[uvw]}$	$d^{G}_{[uvw]}$	α, deg	$d^{AlN}_{[hkl]}$
1	P_4: $(1\bar{2}12)$ and AlN	$[10\bar{1}0]$	[0101]	0.311	0.3597	0	0.311
2		$[10\bar{1}1]$	$[\bar{2}121]$	0.5871	0.6095	4°11'9'	0.5855
3		$[1001]$	$[\bar{2}020]$	0.498	0.492	0	0.498

5. RESEARCH METHODOLOGY

An in-depth SEM study was carried out on different eutectic Fe-C-Si alloys produced from irons of commercial compositions with various amounts of titanium.

5.1. EXPERIMENTAL STRATEGY

This investigation was carried out on hypoeutectic, eutectic and hypereutectic irons whose main difference was mainly, the type of graphite and the level of titanium in the base metal. The study has focused on spheroidal graphite (SG), but some researches based on lamellar graphite (LG), compacted graphite (CG) and superfine graphite (SIG) irons, have been realized too.

All the heats were produced in a 100kg medium frequency induction furnace (250Hz, 100kw) in TQC TECHNOLOGIES (Thermal Quality Control) a spin-off of Fundación Azterlan placed also in Durango (Spain). The charge for each heat consisted of different kg of ductile iron returns and of high purity irons depending on the research. Particular amounts of a commercial graphite (98.9wt.%C, 0.03wt.%S) and of FeSi alloy (74.6wt.%Si, 0.3wt.%Ca, 0.7wt.%Al) are also added to metallic charges. After melting, the composition is checked and finally adjusted according to the required target.

After superheating above 1500ºC, the iron was transferred into the pouring ladle for Mg treatment (when it was necessary) with different quantities of a FeSiMg alloy (47.2wt.%Si, 6.02wt.%Mg, 1.15wt.%Ca, 0.24wt.%Al, 0.30wt.%Mn and 0.88wt.%RE) by the sandwich method (0.55kg for CG, 1.2kg for SG with 1.1wt.% of the batch weight). The FeSiMg was positioned at the bottom of the ladle and the covered with steel scrap, before tapping the melt form the furnace.

For each heat, different thermal analysis cups were poured, and the cooling curves were recorded with the Thermolan® system [40], which is a predictive system of metallurgical quality for spheroidal, lamellar and compacted graphite, prepared to work continuously in aggressive environments.

Inoculation was made directly in the cups by the addition of 0.2% of different commercial inoculants, depending on the study. The solidification of the iron in the cup was interrupted by quenching in brine at increasing times (Figure 9), in order to prevent excessive growth of graphite and to obtain information on the microstructure evolution at various stages during solidification. After cooling to room temperature, the cups are sectioned and prepared for metallographic examination.

To identify possible nucleation sites an Ultra PLUS Carl Zeiss SMT (0.8 nm resolution at 30 kV) in the STEM mode was used in combination with an X-Max 20 Oxford Instruments EDX detector with a resolution of 127 eV/mm2. This investigation was complemented with spectrums (concentration of the X-ray signal in a point), mapping (gives information on the X-ray intensity distribution over the selected region of the sample) and line scans (utilizes the X-ray signal from a specified energy range along any

line in order to show the elements distribution), to analyze the main elements present in the inclusions and to estimate their chemical composition.

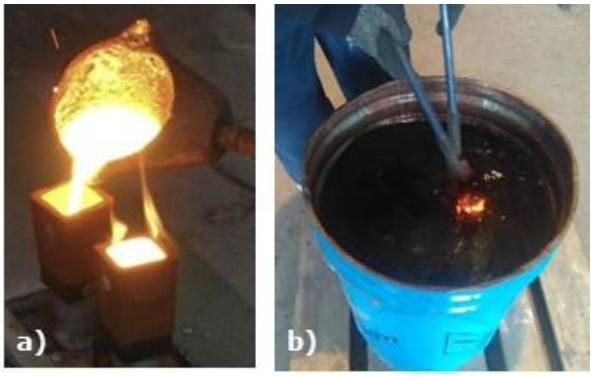

Figure 9. Interrupted solidification experiments: a) thermal analysis cups; b) quenching in brine.

5.2. EXPERIMENTAL RESULTS. LAMELLAR GRAPHITE

Five different heats were produced in our 100kg medium induction furnace. From each melt, six standard (non-tellurium) thermal analysis cups were poured and the cooling curves were recorded. Inoculation was made directly in the cups through the addition of 0.2% of a commercial inoculant rich in Zr and Mn, whose composition is summarized in Table 7.

Table 7. Chemical composition (%mass) of the inoculant.

REF.	Si	Al	Ca	Mn	Ti	Zr	Ce	Ba	Mg	Bi
ZrMn	62.6	1.01	1.79	5.96	0.13	6.77	<0.05	0.65	0.22	<0.02

The chemical analysis of all experimental irons and the graphite morphology is reported in Table 8. For the Ti containing irons, the Mn/S ratio was relatively constant at about 50. For the no-Ti samples this ratio had three different levels [41].

Table 8. Chemical composition (mass%) of experimental cast irons.

HEAT	GRAPHITE	C	Si	CE	Mn	P	S	Ti	Mn/S
Q1SIG	LDG, SIG	2.94	1.92	3.50	0.58	0.022	0.011	0.180	52.7
Q2SIG	SIG	3.10	1.85	3.64	0.53	0.021	0.011	0.320	48.2

Q3LDG	LDG	3.07	1.91	3.59	0.57	0.014	0.011	0.014	51.8
Q4LDG	LDG	3.07	1.91	3.60	0.55	0.015	0.028	0.013	19.6
Q5LAG	LAG	3.02	1.90	3.55	0.53	0.019	0.120	0.013	4.4

The standard graphite (Gr) shapes summarized in Table 8 are uniformly distributed type-A (LAG), interdendritic type-D (LDG) and superfine interdendritic graphite (SIG). This SIG is short (10-20 µm) and stubby, exhibiting rounder edges than type-D, similar to the coral graphite. It is obtained in low-S and moderate-Ti additions (*e.g.* <0.01%S, 0.3-0.4%Ti) irons [42].

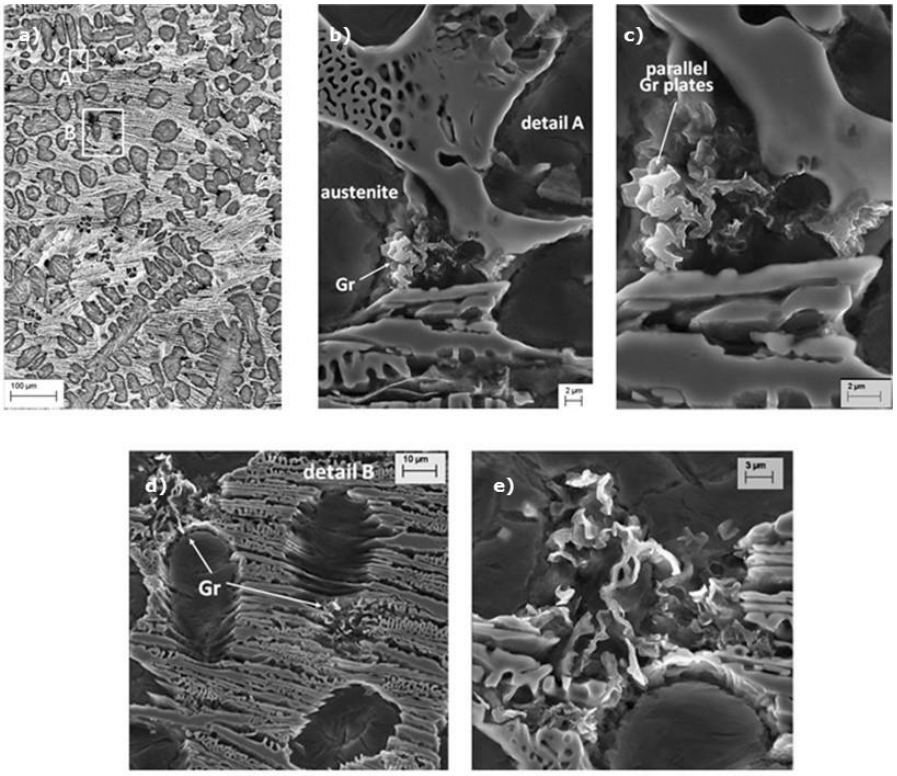

Figure 10. Solidification SEM images for Q1SIG: a) graphite always in contact with austenite at low magnifications; b) detail A: graphite nucleation and growth at austenite/liquid interface; c) higher magnifications of detail A, growth of parallel graphite plates; d) detail B; e) higher magnifications of detail B [44].

In SIG irons (heats Q1SIG and Q2SIG) graphite nucleate at the austenite (martensite)/liquid (γ/L) interface in regions enriched in carbon because of carbon rejection by the austenite and then grow into the liquid (carbides) (Figure 10a,b). Parallel graphite plates emerging from the γ-phase are seen on Figure 10c, which suggests a cooperative γ - Gr growth into the liquid. The orientation of the Gr in the proximity of the austenite, seems

to favor a direction parallel to the γ/L interface (Figure 10d,e). These Gr aggregates then grow into the liquid as spherical graphite/austenite grains.

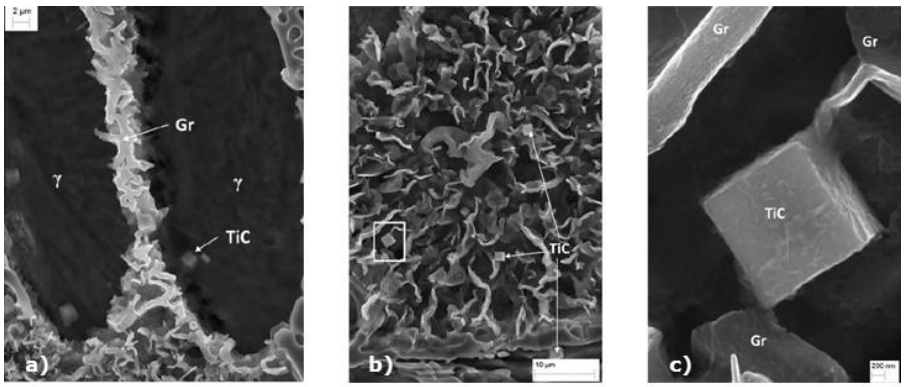

Figure 11. SEM images from heat Q1SIG (0.18%Ti): a) austenite/graphite interface and TiC in the austenite; b) TiC in the γ/Gr eutectic grains; c) TiC in contact with graphite lamellae.

A significant number of titanium carbides (TiC) were observed in the microstructure (Figure 11a). Although they are mostly positioned in the austenite dendrites, there are some evidences of their direct contact with the graphite (Figure 11b,c). Stefanescu et al. [43] found also numerous cuboidal TiC in contact with the graphite, but the authors were uncertain that this was enough proof to accept the nucleation effect of the carbides. According to these new findings, it seems reasonable to assume that cuboidal TiC carbides act as graphite nuclei. On the other hand, no MnS were observed.

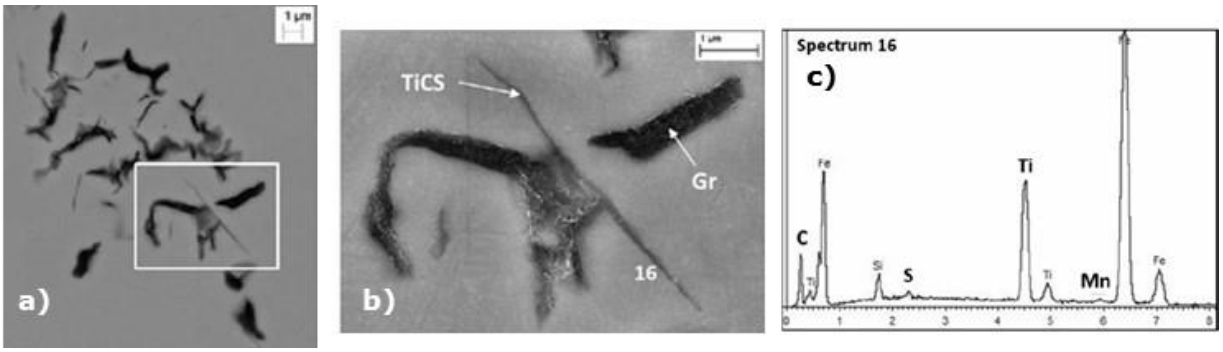

Figure 12. SEM images from heat Q2SIG (0.32%Ti) without etching a) graphite and titanium carbides at low magnifications; b) TiCS needle at higher magnifications: c) WDX/SEM spectrum of the TiCS needle [41].

Complex titanium inclusions were also observed at the higher level of 0.32%Ti (Q2SIG). They were identified firstly in metallographic samples not etched with an evident acicular morphology (Figure 12a,b). As shown by the spectrum of these inclusions in Figure 12c, they seem to contain some S and Mn, referring to them as TiCS needle-like carbides to distinguish them from the cuboidal TiC carbides. They are always in contact with the graphite. This detailed SEM study did not find any MnS acting as

nucleation sites for the low sulfur SIG, so it is possible that the TiCS inclusions serve as nuclei for graphite.

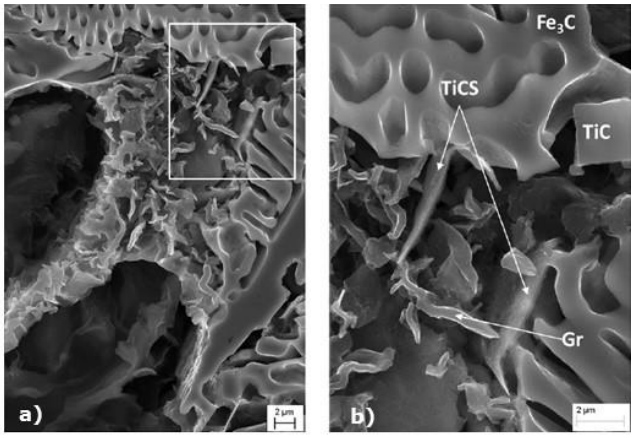

Figure 13. Deep etching SEM images of TiCS needles of iron Q2SIG (0.32%Ti) at different magnifications: a) low; b) high [41].

These needle-like carbides were not detected previously [44] because after deep etching they can be confused with the graphite. However, after their existence was documented from non-etched samples, it was possible to identify them on deep-etched SEM samples (Figure 13a,b).

For the low-S no Ti addition heat Q3LDG, the distribution of the graphite is similar to that in the SIG irons, but the morphology is different. The graphite plates are larger compared to that in SIG (Figure 14b). No titanium carbides were observed in this iron, something expected because of the low percentage of Ti (0.014%). Thus, it is reasonable to assume that nucleation occurs at the austenite/liquid interface (Figure 14a) in regions enriched in carbon, because of carbon rejection by the austenite during solidification. This assumption is in line with the fact that graphite additions are a potent nucleant in lamellar graphite iron.

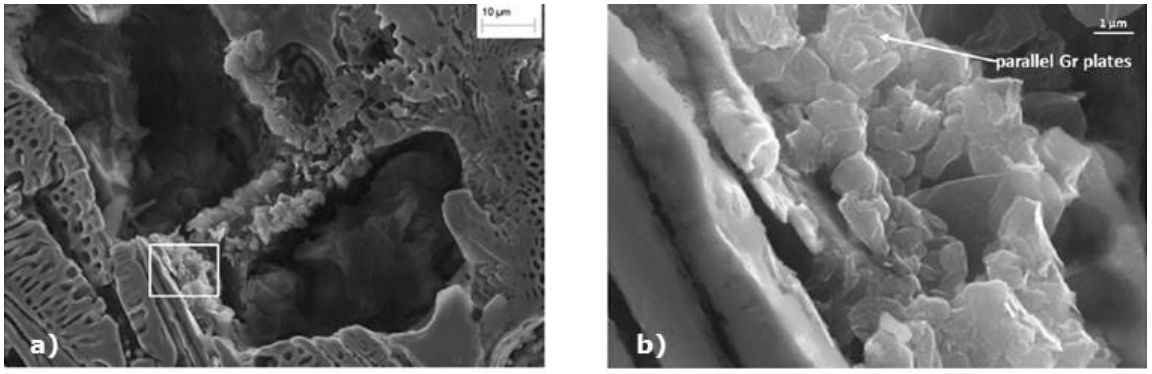

Figure 14. Early solidification for the low-sulfur no-titanium addition iron Q3LDG (0.011%S, 0.014%Ti) at different magnifications: a) low; b) high [41].

The morphology of the graphite in the medium sulfur (0.028%S) heat Q4LDG is similar to that in heat Q3LDG that is type-D, but the graphite is slightly larger, with a more chaotic distribution and with more varied shapes. Again, graphite nucleates at the austenite/liquid interface, but also sometimes on MnS.

The last heat, Q5LAG, which is high in sulfur (0.12%S), exhibits graphite with a totally different morphology type A, more uniformly distributed, with higher aspect ratio and less roundness (Figure 15a). Numerous MnS inclusions, which exhibit a variety of shapes, from polygonal to plates, were observed. Not all of them are graphite nuclei, but when they are (Figure 15b,c), the graphite envelops the MnS inclusions and then starts branching (Figure 16).

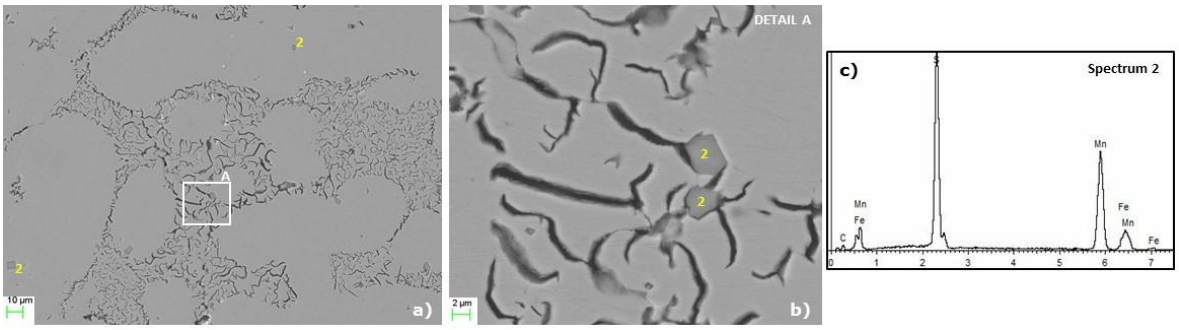

Figure 15. Early solidification for the high-sulfur no-titanium addition iron Q5LAG (0.12%S, 0.013%Ti): a) general microstructure non-etched; b) detail of the graphite nucleating on MnS inclusions; c) WDX/SEM spectrum of MnS.

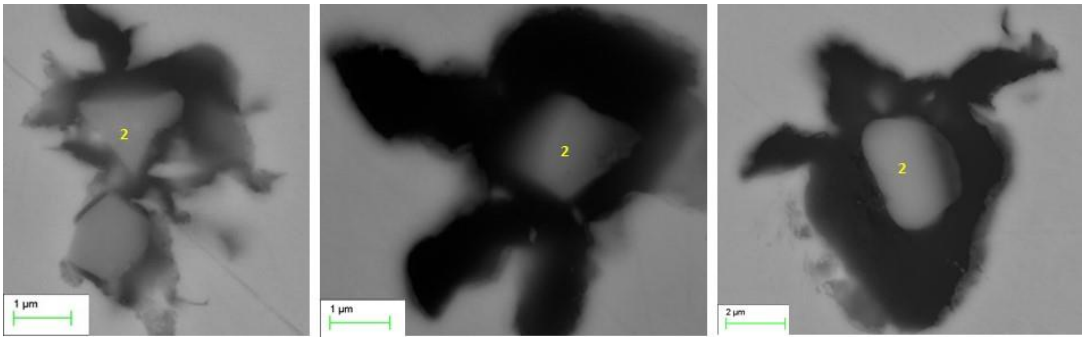

Figure 16. Branching of graphite around MnS nuclei [41].

5.2.1. INFLUENCE OF THE ADDITION OF SULFUR

From the experimental results studied, it is possible to confirm, that in unalloyed very low sulfur irons (0.011% S) with high Mn/S ratio (51.8) interdendritic graphite type-D nucleates at the austenite/liquid interface where carbon rich regions are generated by carbon rejection from the solidifying austenite. As the sulfur content increases to 0.028% and the Mn/S ratio decreases to 19.6, most type-D graphite nucleation continues to occur at the γ/L interface. However, limited nucleation can also take place on MnS inclusions.

At high sulfur contents (0.12% S) and low Mn/S (4.4), both nucleation pattern and graphite shape change drastically. The MnS inclusions exhibiting a variety of shapes become the main source for lamellar type-A graphite nuclei. The graphite grows by first enveloping the inclusions and then branching out in the liquid. Some complex oxides or/and-sulfides of Zr, Al, Mg, Mn and Ca were found acting as nucleation sites for these MnS (Figure 17). This assumption is verified by other researchers [45]. Their values of melting points and free energies of formation (Table 2) makes them perfect candidates to form in the melt.

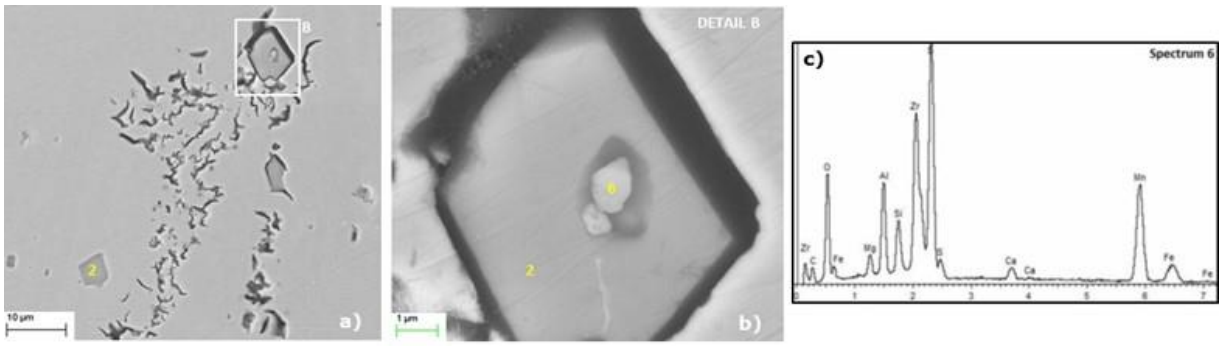

Figure 17. Nucleation and growth of lamellar graphite in heat Q5LAG (0.12%S): a) low magnifications; b) detail of the graphite nucleating in a MnS with other nuclei; c) WDX/SEM spectrum of complex oxides and sulfides [41].

5.2.2. INFLUENCE OF THE ADDITION OF TITANIUM

The addition of titanium to the iron affects significantly both graphite shape and graphite nucleation. In the very low sulfur iron (0.011% S) the graphite changes from interdendritic type-D to superfine interdendritic SIG (Figure 18). While most of the graphite nucleation still occurs at the γ/L interface, some nucleation on cuboidal TiC was also observed.

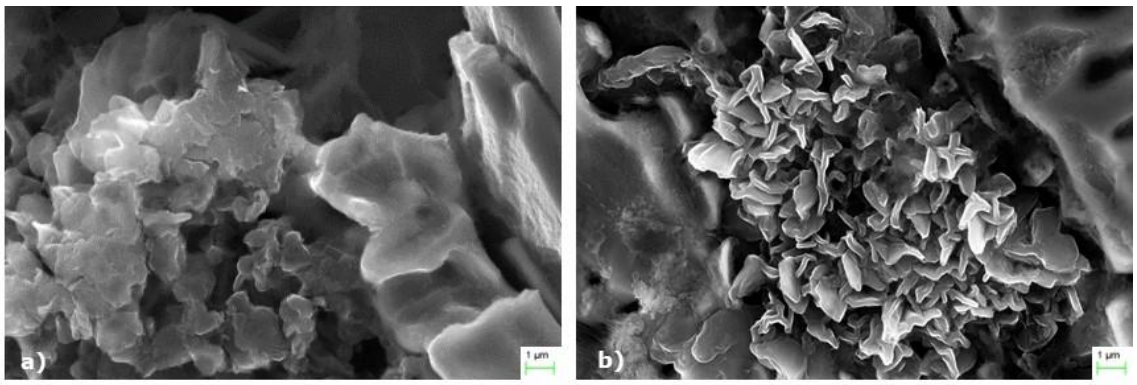

Figure 18. Graphite shape in function of the percentage of Ti: a) Q3LDG (0.014%Ti); b) Q1SIG (0.18%Ti).

Increasing the Ti level to 0.32% at the same sulfur content does not seem to produce significant changes in the microstructure, with the exception of the formation of needle-like complex Ti-C-S-Mn compounds which usually are in contact with the graphite offering the possibility to act as nuclei.

5.2.3. INFLUENCE OF THE NUCLEI ON THE GROWTH OF GRAPHITE

As it has previously discussed, the possibility to find some non-metallic inclusion acting as nucleation site for graphite in irons with low percentage of sulfur is limited. This situation is totally different when this level of sulfur increases and for heats with 0.12%S, the MnS are the main nuclei for graphite. These Mn sulfides present a clear polygonal shape (rectangular, triangular, pentagonal) as it is shown in Figure 19. They seem to play an important role in the growth of graphite, because, according to the pictures, in the early stages of solidification the graphite precipitates around them following faithfully the shape of inclusions, determining the directions of growth.

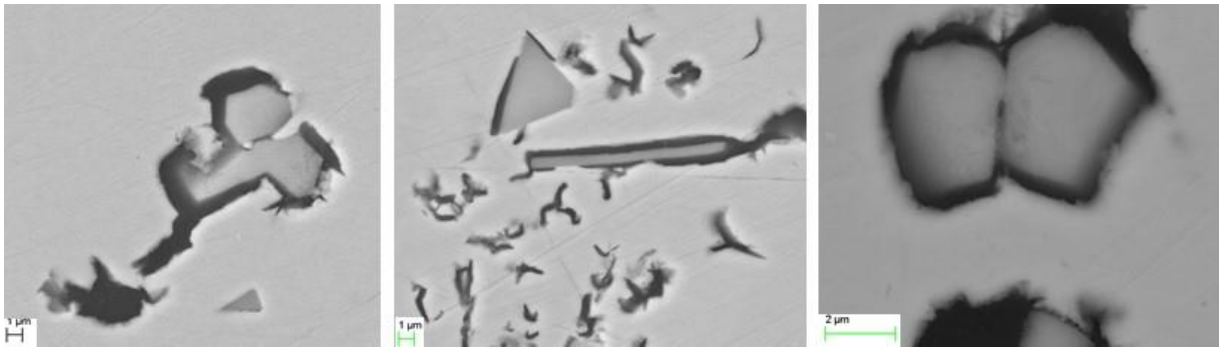

Figure 19. Different shapes of MnS inclusions in heat Q5LAG (0.12%S).

5.3. EXPERIMENTAL RESULTS. TADPOLE GRAPHITE

Three heats were produced in a 100 kg medium frequency induction furnace. From each heat six standard thermal analysis (TA) cups were poured. As always, inoculation has been made directly in the cups with 0.2% of a commercial inoculant, whose composition is summarized in Table 9.

Table 9. Chemical composition (%mass) of the inoculant.

REF.	Si	Al	Ca	Mn	Ti	Zr	Ce	Ba	Mg	Bi
CeBaBi	70.00	0.82	1.49	0.15	0.10	0.05	0.20	0.53	<0.10	0.35

The chemical composition of the three experimental heats and the graphite morphology on the cups that were cooled without quenching is given in Table 10. Some typical microstructures at the end of the solidification for the three heats are given in Figure 20.

Table 10. Chemical composition of cast irons and general microstructure.

REF.	GRAPHITE	CHEMICAL ANALYSIS, wt%							MICROST.
		C	Si	CE	Mn	P	S	Mg	
Quench1	CG+SG	3.69	2.00	4.29	0.14	0.016	0.014	0.022	CG+40%SG
Quench2	CG+SG	3.68	2.14	4.32	0.14	0.016	0.014	0.020	CG+20%SG
Quench3	LG+SG	3.77	2.23	4.44	0.14	0.015	0.015	0.013	LG+SG

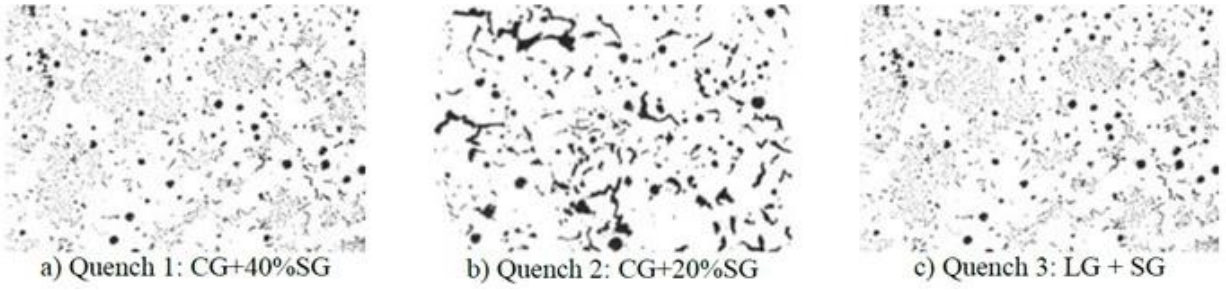

Figure 20. Typical microstructures at the end of solidification.

A new type of graphite is described, known as tadpole graphite (TPG), a term introduced to describe a graphite spheroid that has developed one or more tails which defines the beginning of the transition from SG to CG, as shown in Figure 21.

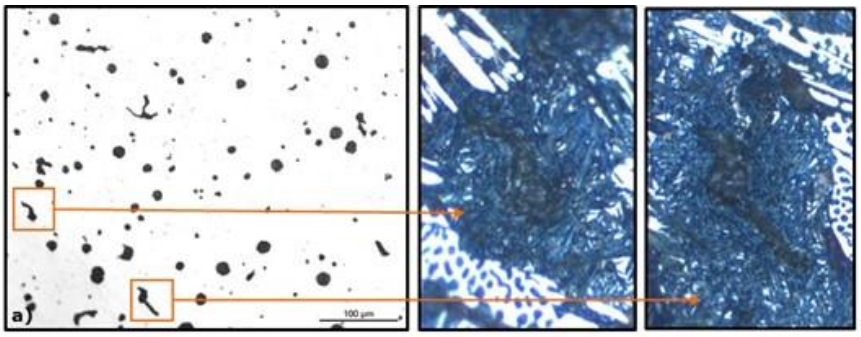

Figure 21. Tadpole graphite formation in a quenched specimen: microstructure in 2D, non-etched (left) and etched with nital (right).

Typical SEM micrographs of tadpole graphite are presented in Figure 22. In this case, two tails have been developed, both of them with different orientations. A clear transition zone is observed too. In this region, where the SG starts generating tails that become CG, branching of graphite appears to occur through twin boundaries defects that result in the splitting of the lamellae along the basal plane [29].

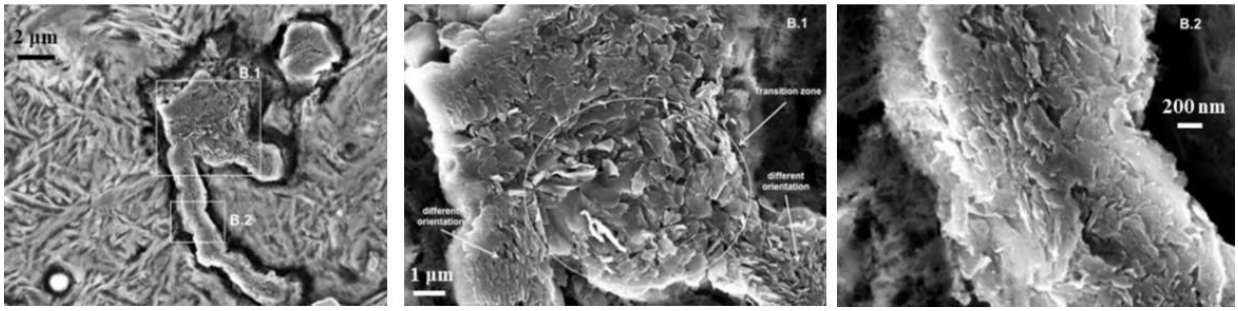

Figure 22. SEM microstructures of tadpole graphite (from Quench2).

At low Mg contents of 0.013%, insufficient for CG formation, the LG in the eutectic colony is highly curved, while the quenched liquid exhibits graphite spheroids (Figure 23a,b). Graphite growth continues to proceed along the (0001) plane but extensive curving of the plate occurs through a fault of low angle boundary or twin (Figure 23c).

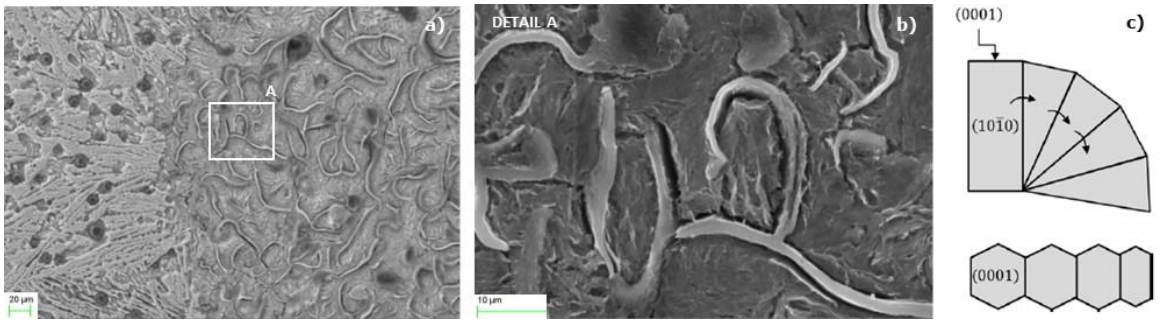

Figure 23. Highly curved lamellar graphite from Quench3: a) general microstructure with some lamellae connected to a rather compacted graphite; b) detail of the beginning of graphite splitting; c) scheme of the curved growth of graphite by a fault of low angle boundary or twin.

Considering these results, the sequence of graphite shape, which changes with increasing Mg, can be postulated as follows. As Mg is added to the melt in amounts roughly under 0.015% the graphite planes start splitting through twinning or twisting of the planes as shown schematically in Figure 24. The surface of the graphite becomes rough with planes protruding and growing in different directions. This curved graphite growth, driven by minimization of surface energy, produces highly curved graphite lamellae as typical for highly undertreated irons.

As the Mg content increases in the range typical for CG iron (0.018-0.022%), in addition to the twining faults, rotational stacking faults occur. A large number of thin or thick plates of various orientations are generated (Figure 22). As the Mg further increases, curved graphite growth becomes dominant

generating spheroidal graphite through one of the two mechanisms, circumferential growth (cabbage model) or conical-helix growth (cauliflower model).

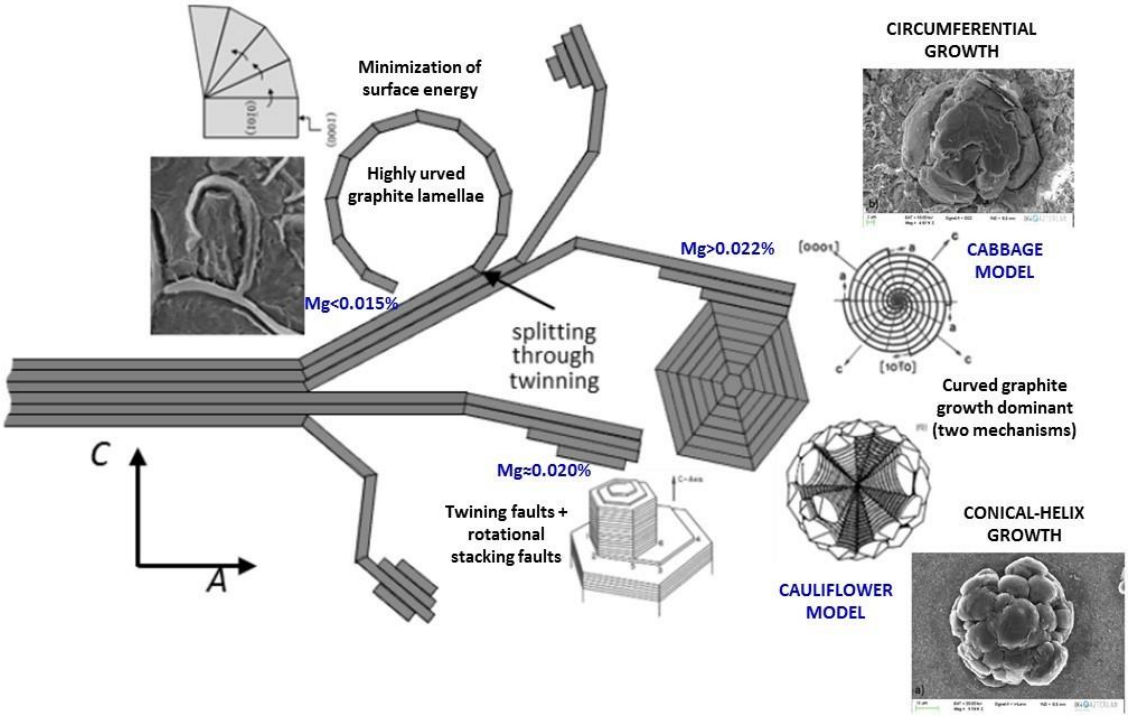

Figure 24. Sequence of graphite formation according to Mg content.

5.4. EXPERIMENTAL RESULTS. COMPACTED GRAPHITE

Three heats with different titanium contents (0.008, 0.019 and 0.0037 mass%) were produced in a 100kg medium frequency induction furnace. The chemical compositions of the experimental heats are presented in Table 11.

Table 11. Chemical composition (mass%) of experimental cast irons.

C	Si	Mn	P	S	Mg	Ti
3.57	2.03	0.15	0.012	0.005	0.014	0.008
3.63	2.06	0.15	0.015	0.006	0.017	0.019
3.64	1.97	0.16	0.012	0.005	0.014	0.037

A total of 27 standard thermal analysis (TA) cups were poured from the melts (eighteen inoculated and nine not inoculated). Inoculation was made directly in the cups through the addition of 0.2% of two different commercial inoculants whose compositions are summarized in Table 12.

Table 12. Chemical composition (%mass) of the inoculant.

REF.	Si	Al	Ca	Mn	Ti	Zr	Ce	Ba	Mg
Ce	70.6	0.87	1.08	0.20	0.06	0.10	1.61	<0.10	<0.10
ZrMn	62.6	1.01	1.79	5.96	0.13	6.77	<0.05	0.65	0.22

The liquid treatment of the various TA cups and the amount of Ti in the base iron are shown in Table 13. The solidification of the iron was interrupted by quenching in brine at increasing times for eighteen of these TA cups, to obtain information on the microstructure and on the nucleation sites at various stages during the solidification (immediately after pouring and after 60 seconds).

Table 13. Liquid treatment of TA cups.

HEAT	%Ti IN THE MELT	INOCULANT	Nº OF NUCLEI
1	0.008	None	25
		Ce	21
		ZrMn	30
2	0.019	None	29
		Ce	33
		ZrMn	50
3	0.037	None	24
		Ce	24
		ZrMn	11

As previously it has been mentioned, an Extensive Field Emission Gun Scanning Electron Microscope (FEG-SEM) examination of the graphite was carried out on non-etched samples. An example of this procedure is illustrated in Figure 25 showing a compacted graphite growing around a complex inclusion from a sample with 0.008%Ti inoculated with the ZrMn inoculant and quenched after 60 seconds.

Three different zones are identified. Spectrum 1 indicates a clear presence of Mg, Si, Al and N. The spectrum for position 2 reveals two clear peaks of Mg and S and two small peaks for Ca and O. Spectrum 3 is very similar but with an important increase in the peak of S and a small peak of La. The analysis of the X-ray composition maps presented in Figure 26 confirms the results suggested by the spectrums, with an important concentration of S, Mg, Ca and O in the core accompanied in one of the corners by an important concentration of Mg, Si, Al and N.

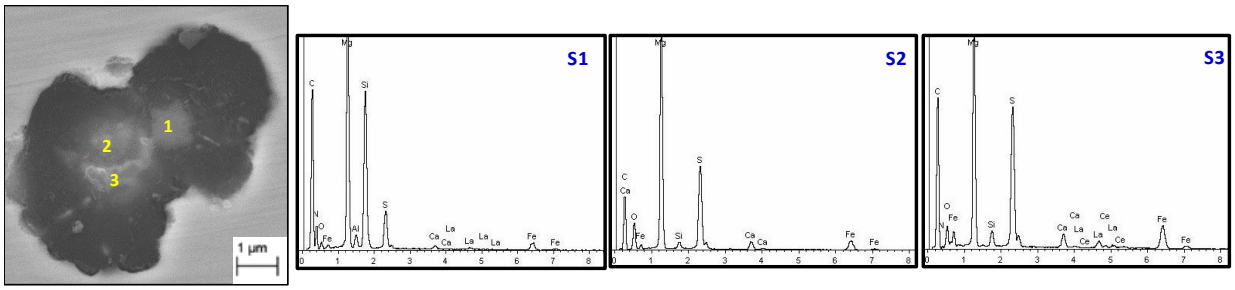

Figure 25. A compacted graphite growing around a complex nuclei and the WDX/SEM spectrums at three different positions on the inclusion.

A more thorough analysis, using X-ray concentration graphs, reveals that Mg, S, Ca and La show composition peaks at the same position (Figure 27). Then, Mg, Si, Al and N also present coincidental maxima. Finally, the O maximum is situated at the same position as the maximum for Mg. Thus, this nucleus appears to be formed by a Mg oxide surrounded by a big rounded Mg-Ca-La sulfide, whose growth was restricted in one direction by a complex (MgSiAl)N.

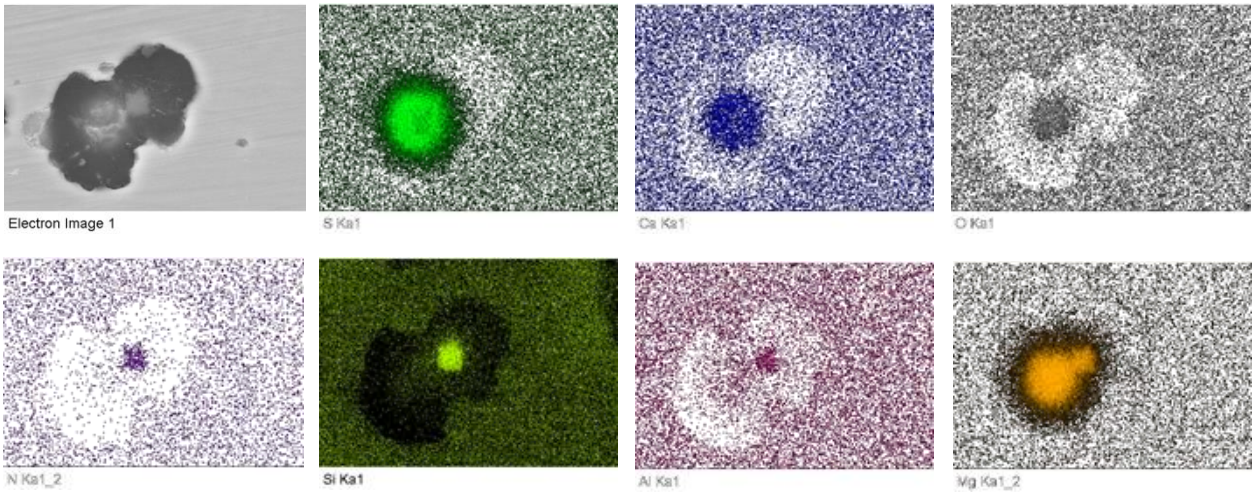

Figure 26. X ray composition maps on the compacted graphite in Figure 25.

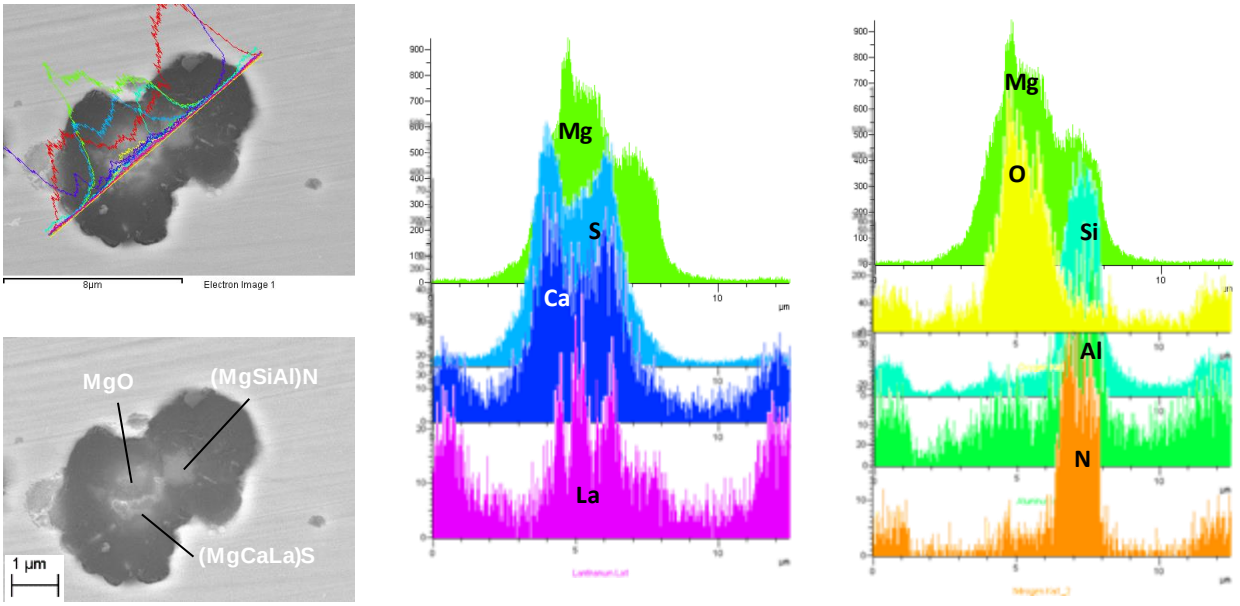

Figure 27. X ray concentration graphs in the compacted graphite in Figure 25.

This procedure is applied in all the graphite studied in this research, and as a result, a summary of the different inclusions detected acting as nucleation sites is shown in Table 14. This summary is function of the inoculant, of the level of titanium in the melt and of the quenching time. It is observed, that sulfides, Mg-Si-Al nitrides, Ti(CN) and oxides, and silicates to a lesser extent, are the main non-metallic inclusions. Principal differences are appreciated in function of the content of titanium.

Table 14. Percentage of inclusions detected in the graphite acting as nuclei.

%Ti IN THE MELT	INOC.	Ti(CN)	(MgSiAl)N	SULFIDES	OXIDES	SILICATES
0.008	none	0%	46%	33%	21%	0%
	Ce	0%	50%	37%	13%	0%
	MnZr	0%	43%	23%	23%	11%
0.019	none	31%	21%	31%	14%	3%
	Ce	21%	37%	27%	15%	0%
	MnZr	35%	20%	34%	9%	2%
0.037	none	50%	0%	50%	0%	0%
	Ce	42%	0%	49%	9%	0%
	MnZr	47%	0%	43%	10%	0%

5.4.1. EFFECT OF THE ADDITION OF TITANIUM IN THE BASE METAL

The Mg-Ca sulfides are the only inclusions detected in all the samples studied in this research, independently of the quantity of titanium present in the base iron. For a 0.037% of Ti, sulfides appear combined with Ti(CN), which seems to restrict their growth in one or several directions (Figure 28).

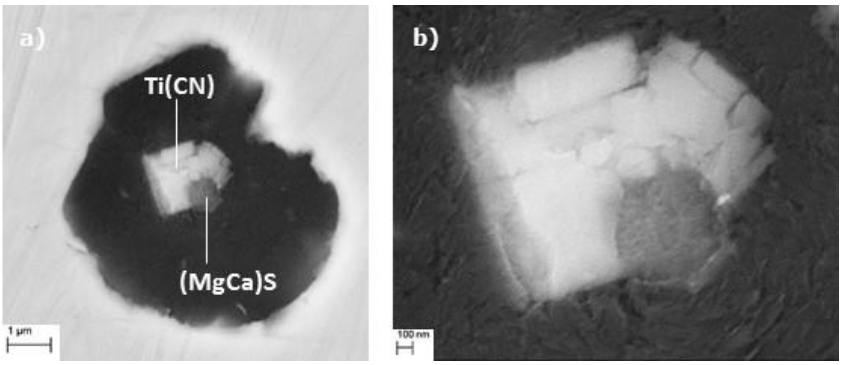

Figure 28. SEM pictures from a sample no inoculated with high percentage of Ti (0.037): a) Ti(CN) restricting the growth of a (MgCa)S; b) detail of the inclusions.

In the case of a low percentage of Ti (0.008%), the sulfides lose their dominance in favor of complex (Mg-Si-Al) nitrides, which do not combine with them. These sulfides seem to have a clear spherical shape, nucleating in some cases on Mg oxides with the same rounded shape (Figure 29). Some RE, specially Ce and La, were detected in sulfides, mainly in their outer shell (Figure 29).

Depending on the content of titanium of the base metal, these sulfides are accompanied by Ti(CN) or (MgSiAl)N, both of them with a clear polygonal shape. Ti(CN) show a shape more cubic (Figure 28a) versus Mg-Si-Al which seems to exhibit more polygonal, large and rectangular(Figure 30a). Both types of nitrides can be detected acting as nuclei for the graphite, and even one for another in the case of Ti carbonitrides (Figure 30a), or in the matrix without any graphite associated (Figure 30b-c). The nucleation efficiency of these nitrides is favored by their crystal structure (based on disregistry calculations previously described).

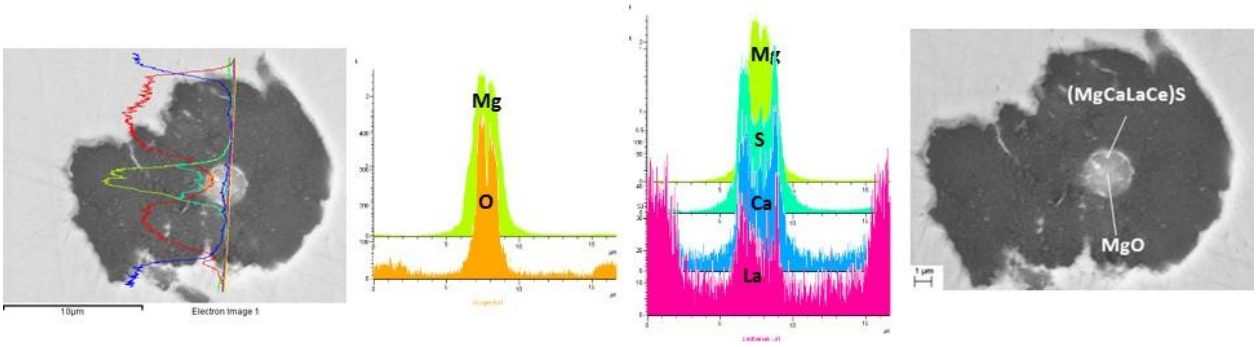

Figure 29. A complex round sulfide nucleating on a MgO, acting both as nuclei for a graphite from the heat with 0.008%Ti.

It is important to note, that although multitude of Mg-Si-Al nitrides have been found alone acting as nucleation sites, there is no evidence of any Ti(CN) as a single inclusion for graphite, and they seems to need always the presence of a sulfide to reveal their nucleation powder (Figure 28).

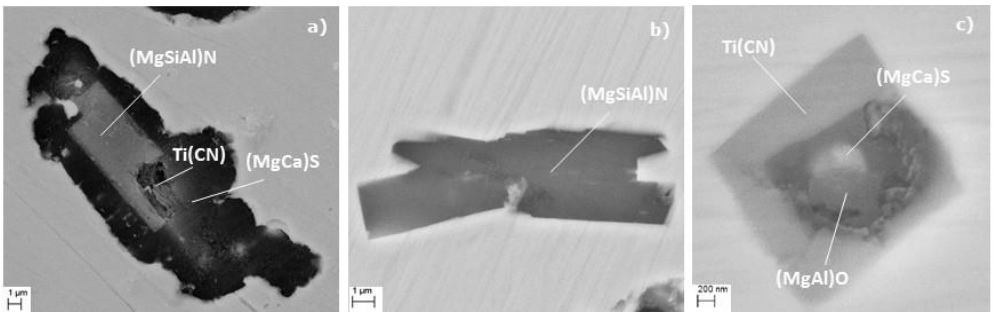

Figure 30. Ti(CN) and (MgSiAl)N non-metallic inclusions: a) acting both as nuclei; b) complex Mg-Si-Al nitride in the matrix without any graphite associated; c) clear cubic Ti(CN) in the matrix.

No (MgSiAl)N were found as nuclei in irons with high percentage of Ti. This is because the high content of titanium does not allow nitrogen to combine with anything else. Something similar happens with Ti(CN) for irons with low level of Ti, what shows the inverse relation between these non-metallic inclusions (Figure 31). Based on these results, it can be concluded that the concentration of titanium in the base metal modifies the preferred nuclei.

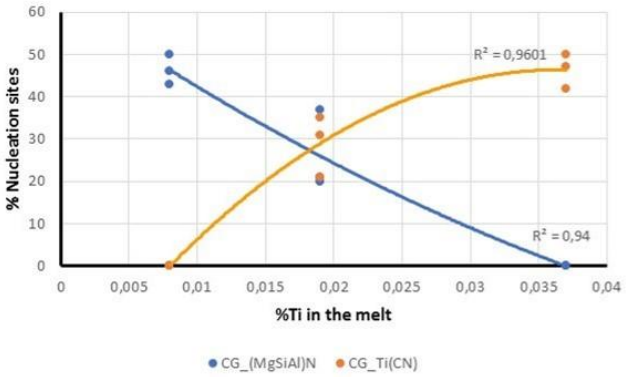

Figure 31. Relation between (MgSiAl)N and Ti(CN) acting as nucleation sites for CG.

Although in a lesser extent, some oxides have been detected acting as nucleation sites for graphite. In most of the cases they are MgO, but some (MgAl)O were also found, overall in irons with high percentage of Ti (Figure 32a).

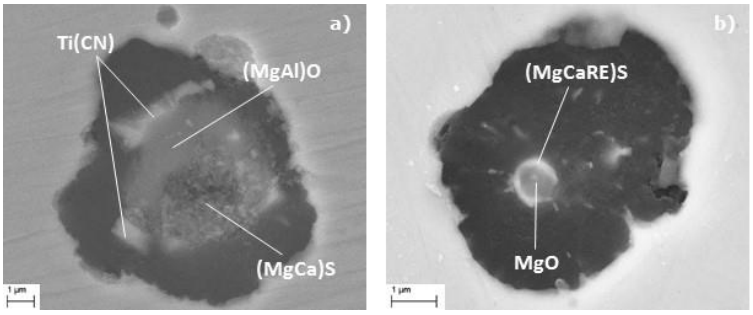

Figure 32. Oxides acting as nuclei for samples inoculated with cerium, quenched after 60 seconds: a) iron with 0.0037%Ti; b) iron with 0.019%Ti.

Oxides were detected practically for all levels of titanium. They are usually rounded (Figure 32b) which implies that they were in liquid state at the time they served as nuclei for other phases, although there are some instances, where they nucleate through all the graphite without any determined shape (Figure 33). It is interesting to emphasize, that the oxides seem to act as nuclei for sulfides (Figure 28,Figure 32) more than direct nucleant for graphite.

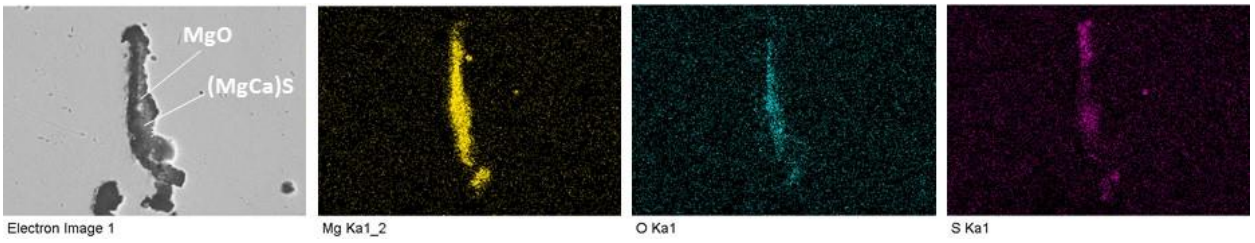

Figure 33. Mg oxide and Mg-Ca sulfide acting as nuclei for a CG (0.008%Ti).

By last, some silicates were observed acting as nucleation site for graphite but only in iron with low or medium content of Ti. Their presence is almost casual, except in sample with 0.008%Ti and inoculated with ZrMn. As a rule, these silicates are rich in Al, La and Ce, and they have been found mainly acting as nucleant for oxides (Figure 34).

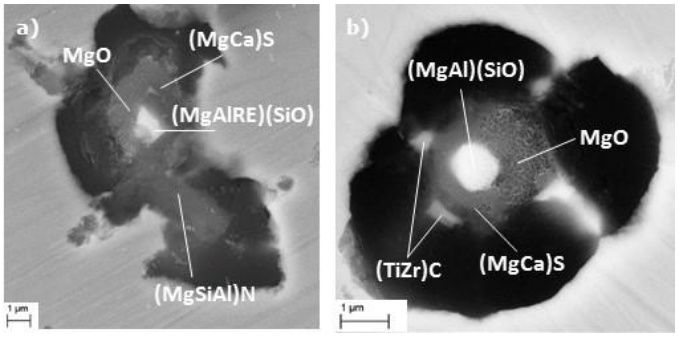

Figure 34. Complex silicates detected in the graphite of irons inoculated with ZrMn: a) low content of Ti (0.008%); b) medium content of Ti (0.019%).

5.4.2. EFFECT OF THE INOCULATION PROCESS

The influence of the inoculation process was studied through the addition of two different type of inoculants, one of them rich in Ce versus the other one rich in ZrMn (Table 12). In general terms, it is possible to conclude that there is no noticeable difference in the type of inclusions generated between inoculated and non-inoculated samples, but there are some issues to note.

5.4.2.1. Ce inoculant

The use of an inoculant rich in Ce does not have a significant effect on the nature of the inclusions detected as nuclei. Because of a smaller interfacial free energy at the nucleating interface [7,8], graphite preferentially nucleates on RE sulfides (Figure 29,Figure 32b) or RE silicates (Figure 34a) over RE oxides during solidification.

The presence of these Mg-Ca-Ce-La sulfides is more related to the quenching time than with the inoculant used. These RE non-metallic inclusions become heterogeneous nucleation sites for graphite during the last stages of solidification [46]. This conclusion is supported by the fact that they are rarely found in nuclei at early quenching time (Figure 35a), while the become usual in nuclei detected at higher solid fractions, independently of the inoculation process (Figure 35b). They could be considered as a second type of nucleation sites that need more time to become activated.

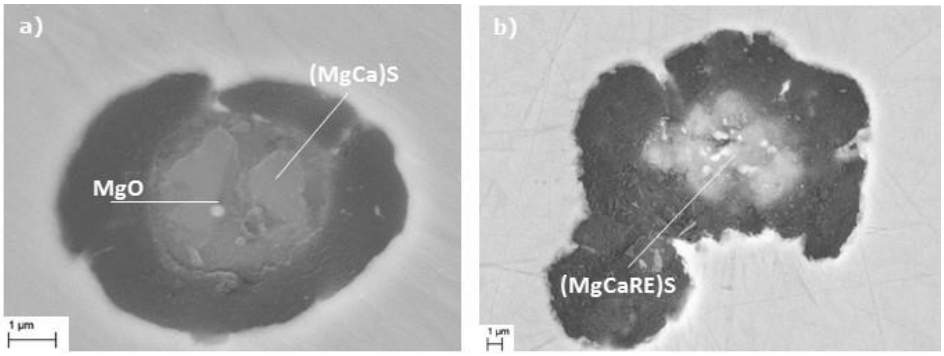

Figure 35. SEM images of graphite with 0.008%Ti: a) sample inoculated with Ce and quenched immediately after pouring (no presence of RE); b) sample not inoculated quenched after 60 seconds (RE as sulfide).

5.4.2.2. ZrMn inoculant

The use of an inoculant rich in ZrMn present disparate results, and its influence depends totally on the content of Ti in the base iron. In this way, the effect of the ZrMn inoculant is clear but only in the samples with medium-high level of Ti, where the majority of Ti carbonitrides are enriched in zirconium. While the affinity of Zr to Ti is obvious to form nitrides, Zr by itself does not react with N or at least the complex Mg-Si-Al combination is stronger to counteract N at low Ti levels, and there is no presence of Zr in any inclusion in irons with 0.008%Ti. There is no evidence of any Mn sulfides.

5.4.3. EFFECT OF THE QUENCHING TIME

The quenching technique used in this research raises the two following concerns: 1) it may cause precipitation of inclusions that will not form during slower cooling; 2) the large undercooling may cause graphite to precipitate on inclusions that have no epitaxy and/or low disregistry with the graphite. However, when samples quenched after 60 seconds (when the eutectic reaction was about half completed) and samples that were not quenched (Figure 36) were analyzed, it was found that the nature of the inclusions was the same, with the only difference of a more common presence of RE elements.

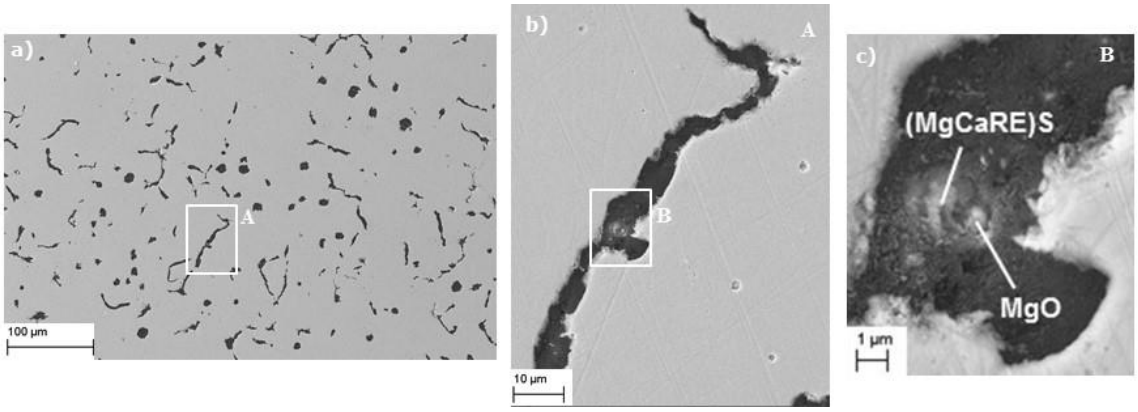

Figure 36. Thermal analysis cup no quenched: a) general microstructure at 400x; b) detail of a compacted graphite with nuclei; c) detail of the nuclei formed by an oxide and a complex sulfide.

5.4.4. INFLUENCE OF THE NUCLEI IN THE GROWTH OF GRAPHITE

Complex Mg-Si-Al nitrides seems to determine the growth the graphite in longitudinal and transversal directions (see arrows in Figure 37), and something similar happens with the sulfides, but indicating a spherical growth concentric to the nucleus [47], with the exception that in this case the growth can be interrupted in some directions by one or more tails (Figure 38). Circumferential growth of the graphite or sectors growing perpendicular to the inclusions faces in the initial stages can explain this behaviour.

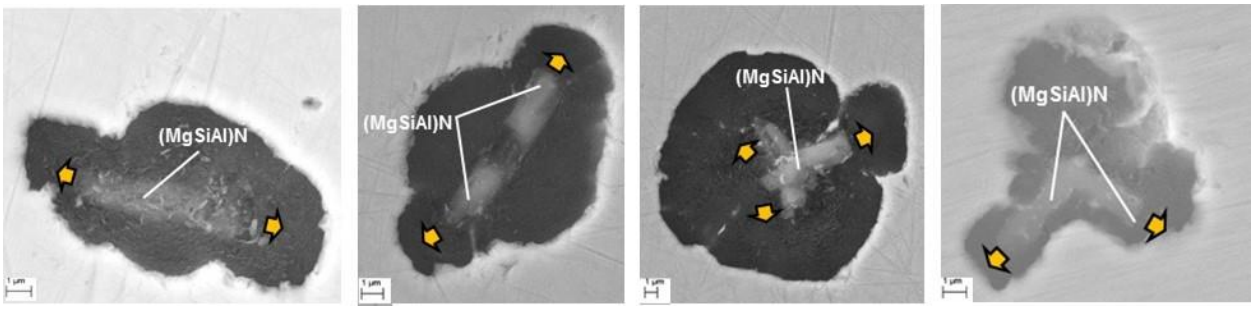

Figure 37. Influence of the (MgSiAl)N in the growth of compacted graphite from the melt with 0.008%Ti.

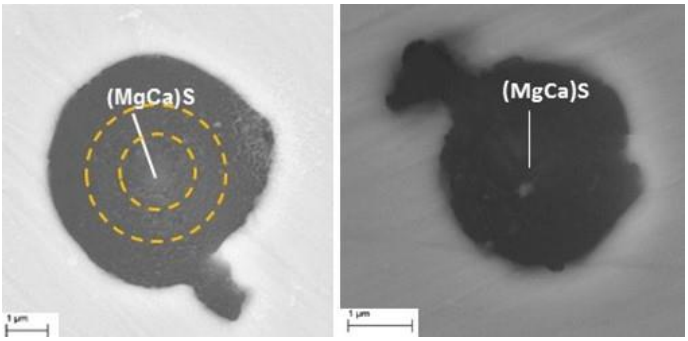

Figure 38. Circumferential growth of compacted graphite (tadpole) around Mg-Ca sulfides from the melt with low Ti.

This direct relation between the type of inclusion and the growth of the graphite disappears when these non-metallic inclusions are combined between them or/and with Ti carbonitrides (Figure 39). According to the previously exposed, the nuclei have a significant effect in the early development of the graphite aggregate, and, when the nucleus is spherical, the platelets are less disorganized as compared with the case of cuboidal or prismatic nuclei. The presence of these inclusions is function of the level of Ti in the base iron, so it is possible to stablish, that the content of Ti in the base metal modifies the nucleation sites but also the growth of graphite.

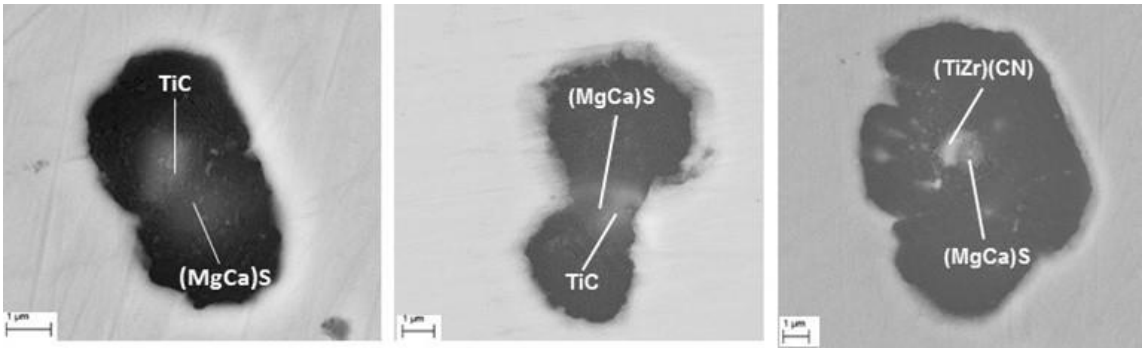

Figure 39. Compacted graphite nucleating in sulfides+Ti carbides inclusions. No evidence relation between nuclei and growth of graphite.

5.5. EXPERIMENTAL RESULTS. SPHEROIDAL GRAPHITE

Six heats with different titanium contents (0.007, 0.011, 0.014, 0.02, 0.03 and 0.036) whose composition is summarized in in Table 15, were produced in our 100kg medium frequency induction furnace.

A total of 32 standard thermal analysis (TA) cups were poured from the melts (twenty-two inoculated and ten not inoculated). Inoculation was made directly in the cups through the addition of 0.2% of

different commercial inoculants whose compositions are summarized in Table 16. The liquid treatment of the various TA cups and the amount of Ti in the base iron are shown in

Table 17. The solidification of the iron was interrupted by quenching in brine immediately after pouring, for sixteen of these TA cups, to prevent excessive growth of spheroidal graphite. After cooling to room temperature, the cups were sectioned and prepared for metallographic examination.

Table 15. Chemical analysis of experimental melts (mass%).

Melt	C	Si	Mn	P	S	Mg	Ti	<0.1%
07	3.69	2.01	0.17	0.016	0.007	0.053	0.007	Cr,Ni,Mo
11	3.75	1.91	0.18	0.021	0.006	0.056	0.011	Cr,Ni,Mo
14	3.68	1.87	0.24	0.005	0.009	0.044	0.014	Cr,Ni,Mo
20	3.30	2.00	0.19	0.018	0.01	0.041	0.020	Cr,Ni,Mo
30	3.78	1.93	0.22	0.016	0.009	0.038	0.030	Cr,Ni,Mo
36	3.55	1.84	0.21	0.023	0.009	0.053	0.036	Cr,Ni,Mo

Table 16. Chemical composition (mass%) of the inoculants.

SYMBOL	Si	Al	Ca	Mn	Ti	Zr	Ce	Ba	Mg	Bi
Al	72.9	3.81	1.42	0.18	0.07	<0.05	<0.05	0.38	<0.10	<0.02
Ti	52.9	1.16	0.89	0.32	9.37	0.06	0.07	<0.1	<0.10	<0.02
BiCe	70.0	0.82	1.49	0.15	0.10	<0.05	0.20	0.53	<0.10	0.35
Ce	70.6	0.87	1.08	0.2	0.06	0.1	1.61	<0.1	<0.10	<0.02
Ba	63.6	1.03	1.21	0.14	0.07	<0.05	<0.05	9.82	<0.10	<0.02
MnZr	62.6	1.01	1.79	5.96	0.13	6.77	<0.05	0.65	0.22	<0.02

Table 17. Liquid treatment of TA cups.

HEAT	%Ti IN THE MELT	INOCULANT	Nº OF NUCLEI ANALYZED
1	0.007	none	9
		MnZr	12
2	0.011	Al	16
		BiCe	16
3	0.014	none	14
		Ti	12
		Ce	11
		Ba	11
4	0.020	none	11
		MnZr	12
5	0.030	none	17
		MnZr	14
6	0.036	none	11
		Ti	12
		Ce	11
		Ba	11

A summary of the different inclusions detected in the graphite nodules as a function of the inoculant and of the level of titanium in the melt is shown in

Table **18**. In general terms, the type of inclusions detected in the core of graphite acting as nucleation sites, are the same as for compacted graphite. Ti carbonitrides, Mg-Si-Al nitrides, sulfides and oxides are the main nuclei and some silicates and phosphides have been detected too. Sulfides and oxides are the only inclusions observed in all samples studied and the presence of Ti(CN) and complex nitrides is totally related to the level of Ti in the base metal (similar to CG).

Table 18. Non-metallic inclusions detected in the graphite acting as nuclei.

IRON	Ti(CN)	(MgSiAl)N	SULFIDES	OXIDES	SILICATES	PHOSPHIDES
07	0%	0%	47%	27%	21%	5%
07MnZr	0%	33%	61%	6%	0%	0%
11Al	0%	36%	44%	12%	0%	8%
11BiCe	0%	30%	48%	19%	0%	3%
14	7%	11%	52%	30%	0%	0%
14Ti	9%	19%	53%	10%	0%	9%
14Ce	0%	37%	42%	21%	0%	0%
14Ba	5%	10%	52%	24%	0%	9%
20	34%	21%	38%	7%	0%	0%
20MnZr	35%	10%	39%	16%	0%	0%
30	38%	14%	43%	5%	0%	0%
30MnZr	37%	5%	58%	37%	0%	0%
36	45%	0%	50%	5%	0%	0%
36Ti	41%	0%	41%	18%	0%	0%
36Ce	48%	0%	48%	4%	0%	0%
36Ba	41%	0%	41%	15%	0%	3%

5.5.1. EFFECT OF THE ADDITION OF TITANIUM IN THE BASE METAL

The main inclusions present in the nuclei in all the samples investigated, independently of the Ti content, were the sulfides. Generally, they are Mg-Ca sulfides which occasionally can present some RE, La and Ce mainly. These inclusions seem to nucleate on oxides and they present usually a clear round shape (Figure 40), according to suggested by Igarashi and Okada [48], who also noted that the spherical shape of the sulfides implies that they were in liquid state at the time they served as nuclei for the other phases.

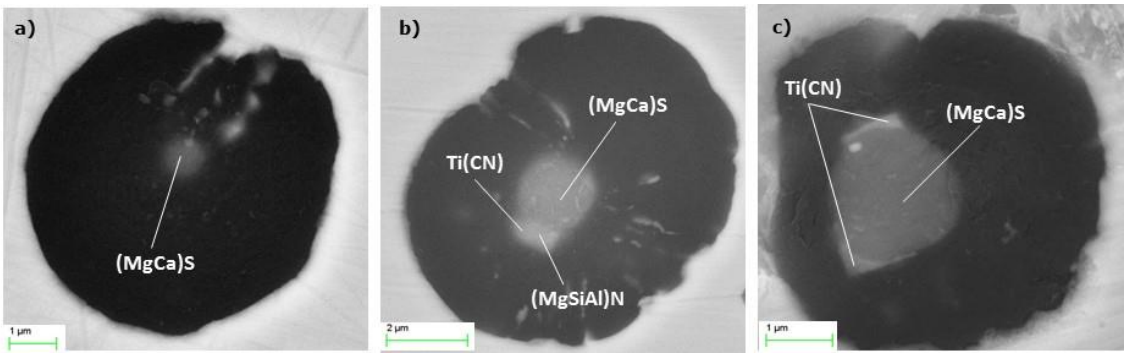

Figure 40. Rounded Mg-Ca sulfides acting as nuclei for samples with different level of Ti in the base iron: a) low Ti; b) medium Ti; c) high Ti.

As a general rule, these sulfides can appear as a single inclusions for low Ti contents (Figure 40a), accompanied by Mg-Si-Al nitrides and Ti(CN) for medium Ti contents (Figure 40b) and only with Ti(CN), for samples with high Ti contents (Figure 40c), which limit their expansion in some directions (Figure 41).

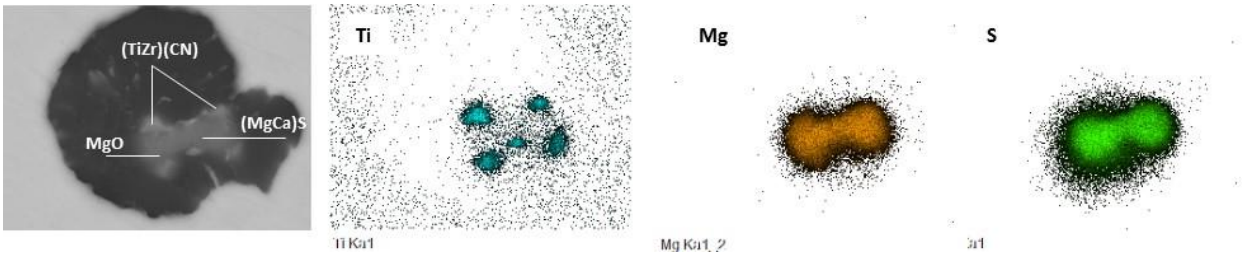

Figure 41. X ray composition maps of a sulfide limited in several directions by Ti-Zr carbonitrides, in a sample with 0.030%Ti inoculated with MnZr.

Both types of nitrides are the second variety of non-metallic inclusion more common acting as nucleation site for spheroidal graphite. Their presence is totally related with the content of Ti in the base metal, keeping an inverse relation between them (Figure 42).

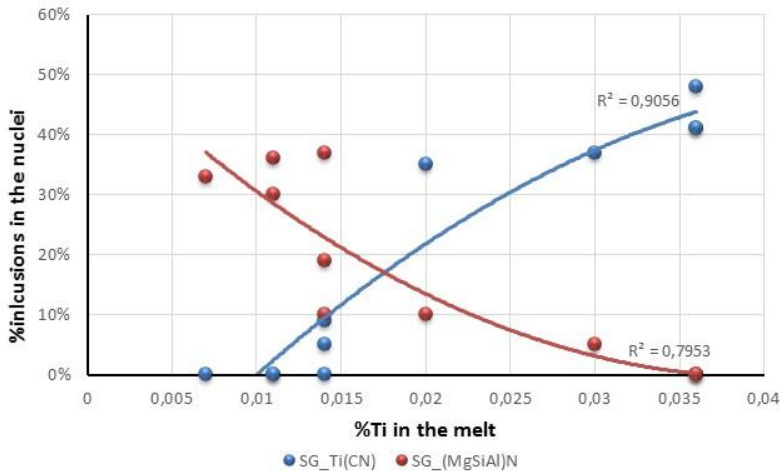

Figure 42. Relation between (MgSiAl)N and Ti(CN) acting as nucleation sites for SG in inoculated samples.

In irons with low percentage of Ti, no Ti(CN) were detected and the number of complex (MgSiAl)N was significant. As the percentage of Ti increases, the number of Ti carbonitrides is enhanced, and the number of complex nitrides decreases, up to a maximum of 0.036% Ti in the iron, where no (MgSiAl)N were found as nuclei. These nitrides present a clear polygonal shape (Figure 43), cubic or even hexagonal, which in principle made them bad nucleants for the graphite although the disregistry calculations previously described, have contradicted this theory. They can appear as a single inclusion (Figure 43a) or combined with other non-metallic inclusion (Figure 43b). In any case, they are much smaller and with shorter length than the nitrides for compacted nitride.

Ti(CN) play also an important role in the nucleation process of SG, overall in all the irons with a high content of titanium in their metals base. Although it is true that some Ti carbides are detected in samples with 0.014%Ti, it is from values close to 0.020%Ti where they acquire a significant relevance. They are perfect nuclei for graphite (something demonstrated by disregistry calculations) but they have never found acting as a single inclusion. This fact highlights the need of a second inclusion where they can nucleate, a sulfide in all the cases studied, which is surrounded total or partially by these Ti(CN), restricting their growth in one or several directions. As it happened with the Mg-Si-Al nitrides, these Ti carbonitrides have a clear cubic shape totally different from the roundness of the sulfides to which they envelop.

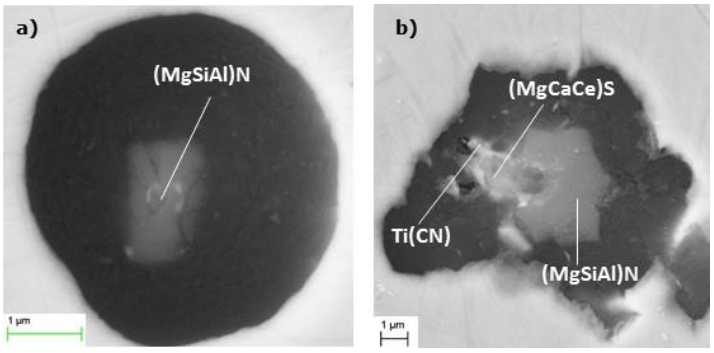

Figure 43. Polygonal Mg-Si-Al nitrides acting as nucleation site in iron with low %Ti: a) as a single inclusion; b) in a complex sequential nucleation combined with sulfides and Ti carbonitrides.

Oxides, are the second type of non-metallic inclusions, present in all the samples analyzed, but their presence is apparently much less relevant than the compounds described so far. They are mainly MgO, although some (MgAl)O were detected too (Figure 44a). Only in one case, an oxide was found acting as a single inclusion for graphite (Figure 44c). In the rest of cases, oxides seem to act as nucleation sites for sulfides, which surrounded them total or partially. For very low levels of Ti (0.007%), these oxides can nucleate in turn, in silicates rich in Mg and Ca (Figure 45a) or even in Al, La and Ce, enveloping totally.

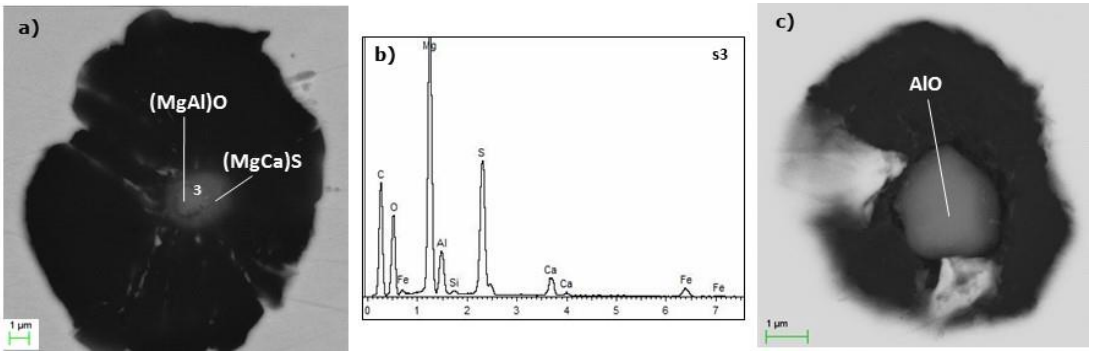

Figure 44. Oxides acting as nucleation sites for graphite: a) (MgAl)O combined with a (MgCa)S; B) WDX/ SEM spectrum on the inclusion in Figure 44a; c) AlO as a single inclusion.

The last type of non-metallic inclusions detected in the graphite were the phosphides, which are rich in cerium and lanthanum (Figure 45c), and more common for low levels of titanium. According to the literature [49], the phosphorous-containing particles result from reactions occurring during the final stages of solidification and are located at the grain boundaries without any graphite associated, but the lack of Ti seems to favor nucleation on them. They do not appear alone but combined with sulfides or complex nitrides.

As it can check with these results, the concentration of titanium in the base metal, in addition to modifying the nucleation sites of graphite, also affects the sequential growth of the nuclei, containing the nucleus multiple compounds that can nucleate on one another:

- Sulfides on oxides on silicates for Ti <0.010%
- Mg-Si-Al nitrides on sulfides on oxides for 0.010%<Ti<0.020%
- Ti(CN) or/and Mg-Si-Al nitrides on sulfides for 0.020%≤Ti≤0.030%
- Ti(CN) on sulfides for Ti>0.030%

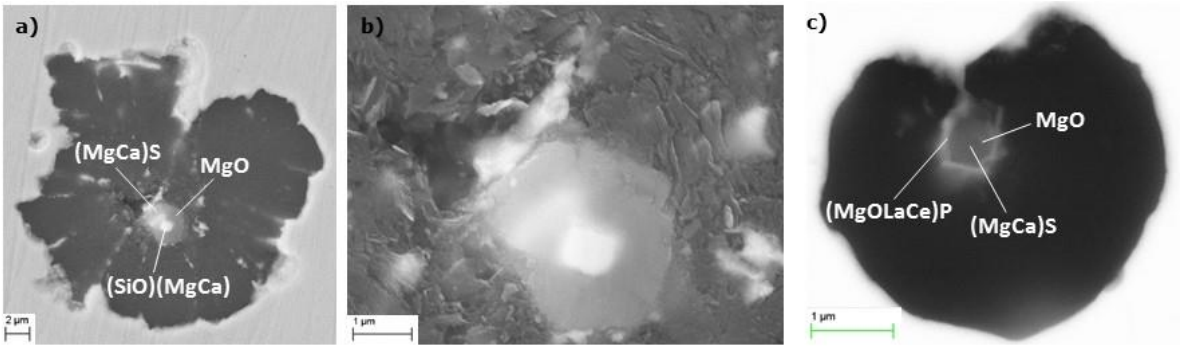

Figure 45. Less common non-metallic inclusions acting as nuclei for graphite : a) silicate accompanied by an oxide and a sulfide; b) detail of the inclusion of the graphite on Figure 45a; c) phosphide accompanied by an oxide and a sulfide.

The last effect of this variation of the Ti content is related to the nodule count and /or eutectic undercooling recorded by the Thermolan®. A summary of the relevant data is included in Table 19. As shown in Figure 46a, higher nodule count results in lower undercooling during the eutectic solidification. For the uninoculated irons, the nodule count exhibits a maximum at a level of 0.03% Ti (Figure 46b) above which the volumetric density of the graphite nodules decreases, probably due to the excess of Ti generates coalescence and inclusions in the matrix without graphite.

Table 19. Nodule count and maximum undercooling temperature for various inoculants.

Iron	T_{E_min}	nod/mm^2
07	-	-
07MnZr	-	-
11Al	-	333
11BiCe	-	341

14	1140	145
14Ti	1149	275
14Ce	1150	352
14Ba	1143	-
20	1142	340
20MnZr	1145	400
30	1144	430
30MnZr	1144	550
36	1134	106
36Ti	1140	179
36Ce	1145	169
36Ba	1138	113

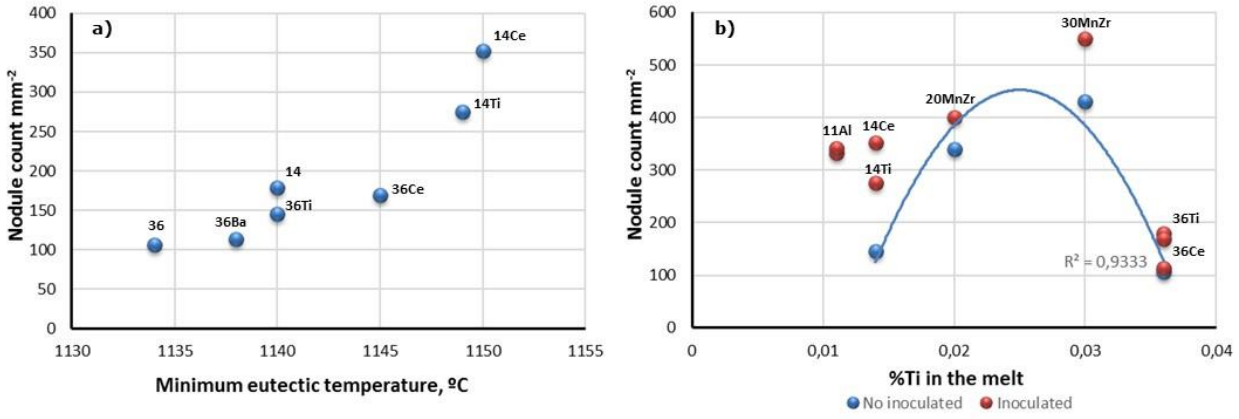

Figure 46. Effect of titanium in the base iron on the eutectic undercooling and on the nodule count.

5.5.2. EFFECT OF THE INOCULATION PROCESS

Although the effect of each inoculant will be studied independently, it is possible to stablish in general terms, that there is no relevant difference in the type of inclusions generated between inoculated and no inoculated samples (

Table 18). On the other hand, the inoculant affects the nodule count, increasing it at all Ti contents (Table 19). Ce inoculant seems to be the most effective for low Ti versus ZrMn inoculant for high Ti, but the influence on the nature of the nuclei is not significant in most of the cases.

5.5.2.1. Ti inoculant

It has been demonstrated that the small changes of the percentage of titanium in the base melt, alters drastically both the type of inclusions on which the graphite nucleates, and the nodule count, but the addition of Ti in the inoculant is totally different and hardly modifies the nature of the nuclei. Some Ti(CN) were detected in samples inoculated with Ti, but their presence is more related to the level of Ti in the iron than with the inoculant used.

5.5.2.2. Ba inoculant

The use of inoculants rich in Ba has been always associated with an improvement of nodule count, nodularity and mechanical properties [50,51]. In this investigation, samples inoculated with that inoculant have not shown any significant increase of volumetric density of graphite and only a rise in the number of phosphides was prominent. Curiously no Ba inclusions were detected in their nuclei. Same conclusions can be applied to Bi inoculant.

5.5.2.3. Ce inoculant

When the samples are inoculated with an inoculant rich in RE, some inclusions with Ce and La are detected. These compounds are mainly sulfides (Figure 47a), although some phosphide has also been observed (Figure 47b). However, some RE non-metallic inclusions were also found in un-inoculated samples (Figure 47c), which suggests that the Ce effect is mostly due to the nodulizing agent, increasing the nodule count.

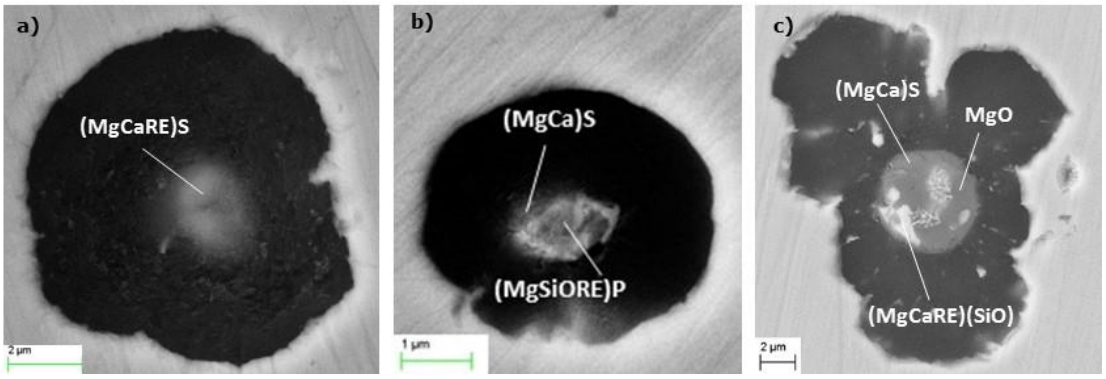

Figure 47. Different types of RE non-metallic inclusions: a) sulfide; b) phosphide; c) silicate.

5.5.2.4. ZrMn inoculant

The influence of ZrMn inoculant is clear, and for irons with a high concentration of Ti in the base iron, as an increased number of carbonitrides was found, all of them were enriched in zirconium, demonstrating the great affinity of Zr to Ti, something similar to what happened in the compacted graphite. There was no detected any inclusion with Mn.

5.5.3. EFFECT OF THE QUENCHING TIME

With the objective to demonstrate that the cooling in water do not have an influence in the type of non-metallic inclusions which can act as nucleation sites for graphite, 3 thermal samples without any quenching were analyzed following the same SEM techniques and summarizing the results in Table 20.

Table 20. Non-metallic inclusions detected in the graphite acting as nuclei for samples no quenched.

THERMALS	Ti(CN)	(MgSiAl)N	SULFIDES	OXIDES	SILICATES	PHOSPHIDES
14	17%	17%	33%	17%	0%	16%
20MnZr	30%	18%	43%	9%	0%	0%
36	33%	0%	33%	27%	7%	0%

As it already happened in the quenched samples, sulfides are the most common inclusions followed by Ti carbonitrides and Mg-Si-Al nitrides depending on the level of Ti. The number of oxides is also relevant, acting always as nucleation sites for the sulfides. Some silicates for the highest level of Ti and some phosphides for the lowest level were detected too. The combination of sulfides+(MgSiAl)N (Figure 48a), sulfides+Ti carbonitrides rich in Zr (Figure 48b), and oxides+sulfides+Ti carbonitrides (Figure 48c) are the typical nuclei for irons with 0.014%Ti, 0.020%Ti and 0.036%Ti respectively, so, in view of these results, the quenching does not seem to have an influence in the nature of nuclei.

Perhaps the most relevant difference over the quenched samples refers to the presence of La and Ce, as phosphides but overall as sulfides, in around 20% of graphite studied, what would demonstrate that they could be considered as a second type of nucleation sites and need more time to become activated (similar to CG). These RE can appear distributed in all the inclusion or only in the periphery of it as a shell.

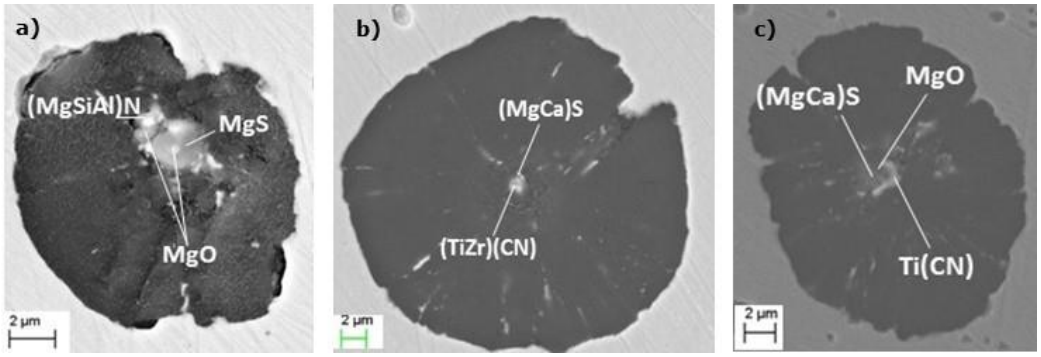

Figure 48. Typical inclusions detected in the graphite of non-quenched samples: a) for 0.014%Ti; b) for 0.020%Ti inoculated with MnZr; c) for 0.036%Ti.

5.5.4. INFLUENCE OF THE NUCLEI IN THE GROWTH OF GRAPHITE

Heterogeneous nucleation is a process that involves two phases with different atomic arrangements coming into contact which causes a certain degree of lattice mismatch between the nucleated solid and the substrate. The magnitude of the mistmatch is, therefore, dependent on the relative crystal orientation of the two phases [52]. Substantial SEM experimental evidences have demonstrated that when the nucleus is spherical, the platelets are less disorganized as compared with the case of cuboidal or prismatic nuclei. Indeed, (MgCa)S nuclei (Figure 49a) promote early envelopment of the inclusion by graphite, and with less defects, than for cubic (TiZr)(CN) inclusions (Figure 49b), or (MgSiAl)N inclusions (Figure 49c).

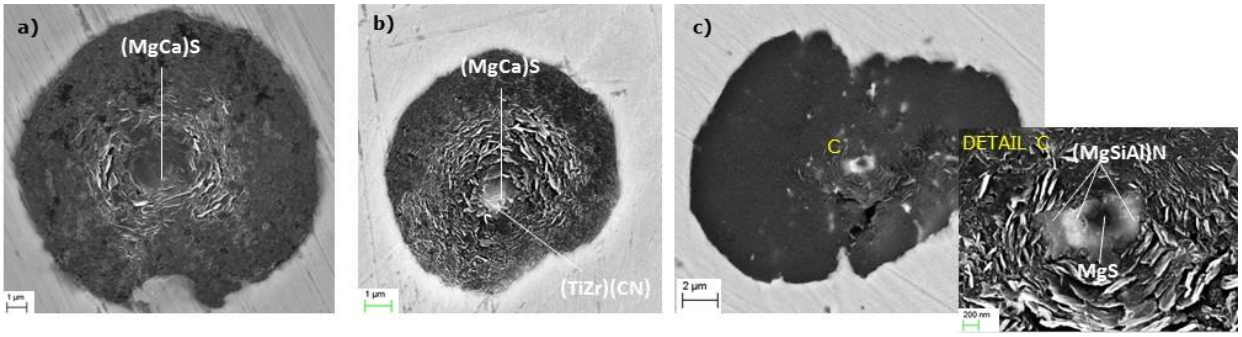

Figure 49. SEM images showing nucleation of graphite platelets: a) on Mg-Ca sulfides in iron with 0.014%Ti; b) on Mg-Ca sulfides and Ti-Zr carbonitrides in iron with 0.020%Ti inoculated with MnZr, c) on Mg sulfides and Mg-Si-Al nitrides in iron with 0.014%Ti.

All these non-metallic inclusions generate an initial disorder that step by step is corrected as the graphite grows (Figure 49). In the case of sulfides, this growth seems to be circumferential and concentric to the inclusion (Figure 49a) ending in a perfect spheroidal graphite. This spherical growth is

also promoted by some Mg-Si-Al nitrides acting alone (Figure 49c), in contradiction to CG where these complex nitrides advanced a clear growth in longitudinal and transversal direction (Figure 37). In general, it could be said, that the single inclusions favor a spheroidal growth independently of the nature of compound. This relation is not so evident when the nucleation sites are more complex because of the addition of inoculant and of the increase of titanium content in the base iron.

6. FINAL CONCLUSIONS

The results of this investigation have demonstrated once again, the enormous complexity of the study of nucleation of lamellar, compacted, but overall, of spheroidal graphite. In order to identify the main compounds acting as nuclei in ductile irons, interrupted solidification experiments (quenchings) at different increasing times were conducted and advanced SEM techniques were used. A series of thermal analysis cups with various percentages of titanium and sulfur in the metal base were poured. These samples were inoculated in several cases with a high variety of inoculants rich in different trace elements (Ce, Ti, Ba, Zr, Al).

The beginning of the transition from SG (spheroidal graphite) to CG (compacted graphite) was stablished by a new category of graphite, called tadpole graphite (TPG) which is a graphite spheroid that has developed one or more tails.

Other intermediate shape has been identified as superfine interdendritic graphite (SIG), characterized by a fine (10-20µm) and highly branched fibrous structure, which nucleates at the austenite/liquid interface, apparently on graphite substrates.

Small variations in the percentages of certain elements (Ti, S) in the base iron modify drastically the nature of the inclusions which can act as nuclei for graphite.

In gray irons with 0.011-0.12%S and 0.013-0.32%Ti, graphite shape is determined by the addition of titanium, changing from SIG to LDG to LAG. Graphite nucleation is mostly controlled by the sulfur level. In low sulfur irons nucleation occurs at the austenite/liquid interface where carbon rich regions are formed because of rejection of carbon by the solidifying austenite and on cuboidal titanium or TiCS needle-like carbides, when the percentage of Ti is high. In the high sulfur irons, nucleation occurs on manganese sulfides, which can nucleate on complex oxides and sulfides.

Both spheroidal and compacted graphite present the same non-metallic inclusions acting as nuclei for graphite. For compacted graphite, MgCa sulfides and (MgSiAl)N nucleating independently, are the main inclusions for the samples with low percentage of Ti. The combination (MgCa)S + Ti(CN), are the typical nucleation sites for samples with high %Ti.

In the case of spheroidal graphite, MgCa sulfides accompanied by Ti(CN), (MgSiAl)N or both, depending on the content of titanium in the iron, were the main inclusions for spheroidal graphite nucleation, regardless of inoculation. Both complex nitrides and carbonitrides seem to restrict the growth of the sulfides increasing the number of nodules. Some silicates and phosphides were found as nuclei but mainly in irons with low content of Ti (<0.014%).

Theories inferring that graphite spheroids nucleate on non-metallic inclusions that contain an MgS core surrounded by an oxide shell, or with an outer shell of complex magnesium silicates, do not, in most cases, explain some of the findings in these works, as in many instances the nucleus was made of two or three different compounds, and all of them were in contact with the graphite.

Mg-Si-Al nitrides and Ti carbonitrides present an inverse relation which is function of the percentage of titanium in the base iron. It is important to note that no Ti carbonitrides were detected alone in the graphite. They need another non-metallic inclusion (usually a sulfide) to act as nucleation site.

(MgSiAl)N and Ti(CN) were proven to be very effective as nuclei for CG and SG. Thermodynamic analysis and disregistry theoretical calculations for both supported this assertion.

The role of nitrogen and titanium in the nucleation of ductile iron appears to be more important than expected, influencing the percentage of Ti in the melt drastically the nature of nuclei.

The inoculation process did not seem to have a significant influence on the type of inclusions at the core of graphite, except for Zr which present a great affinity with the Ti to form carbonitrides.

RE acting as silicates and overall, as sulfides, can be considerate as a second type of sites that are active later during the solidification sequence.

Crystallization of the graphite aggregate evolves through several mechanisms including, foliated dendrite/tiled-roof, curved-circumferential, cone-helix (positive wedge disclination), and helical (negative wedge disclination) growth.

For CG, the effect of the nucleus crystallography on the graphite shape is significant. For (MgSiAl)N and sulfides, there is a clear correlation between the growth of graphite and nuclei: in the direction of the inclusion (in the case of nitrides), circumferential for sulfides. This effect disappears for the Ti(CN). In the case of SG, this relation seems to verify for sulfides, but for the rest of inclusions the tendency is not so evident.

7. ORIGINAL CONTRIBUTIONS AND FUTURE RESEARCH DIRECTIONS

The main novelty of this investigation is given by its own development, where an extensive literature review has been coupled with a series of interrupted solidification experiments and with a complete SEM characterization which has consisted in the use of three different detectors combined with the most sophisticated techniques, as line scans, mappings and spectrums. The use of all these research applications, has allowed promoted some original contributions to the study of the nucleation process of Fe-Si-C alloys.

Two new types of graphite have been identified, tadpole graphite (TPG) and superfine interdendritic graphite (SIG), and their nucleation have been studied.

The role of nitrogen and titanium in the nucleation of spheroidal and compacted graphite appears to be more important than previously thought, altering considerably the type of inclusions on which the graphite nucleate. The content of Ti in the melt changes the preferences of nucleation for graphite (Ti benefits also the multistage sequential growth).

There was no enough literature information supporting the major role of Ti carbonitrides in the nucleation of ductile iron, and they have been found as one of the most important nucleation sites for spheroidal and compacted graphite. Theoretical disregistry calculations have demonstrated, that (MgSiAl)N and Ti(CN) are very good nucleants for graphite.

The importance of (MgSiAl)N as nucleation sites for SG and CG was verified (their existence was known but they were not considered as one the main inclusions for graphite)

The nature of the nuclei is not influenced by the addition of different inoculants, which act directly on the nodule count.

The type of the nucleation site seems to determine the growth of the graphite, overall, in the first instances of solidification.

One of the future research directions would be focused on the study on the nucleation of degenerated graphite such as exploded, chunky or spiky, in order to know which is the nature of the main inclusions that can act as nuclei for these types of graphite and try to avoid them as far as possible.

In the same way, a control of the formation of graphite in those moments of the solidification process where it is more necessary (mainly in the last stages to counteract the formation of microshrinkage) is a key issue to obtain castings free of defects. This is directly related with the nucleation of graphite at the

end of solidification which can be favoured by the addition of some specific inoculants. The search and analysis of those inoculants is another of the fundamental issues to achieve in the future.

8. REFERENCES

[1] F. Campbell, “Elements of Metallurgy and Engineering Alloys”, *Materials Park, Ohio:ASM International,* p. 453, 2008.

[2] D.M. Stefanescu and S. Katz, “Thermodynamic Properties of Iron Base”, *ASM Handbook,* pp. 41-55, 2008.

[3] S. Martin, D. Holmgren and L.S. Ingvar, “Effect of Alloying Elements on Graphite Morphology in CGI”, *5th International Conference on Solidification and Gravity, 4-5th September, Trans. Tech. Publications Ltd,* vol. 649, pp. 171-176, 2008.

[4] K. Cooper and C.R. Loper, “Some Properties of Compacted Graphite Cast Iron”, *Trans. AFS,* vol. 86, pp. 241-248, 1978.

[5] R. Warrick, “Spheroidal Graphite Nuclei in Rare Earth and Magnesium Inoculated Irons”, *AFS Cast. Metals Research J.,* pp. 97-108, 1966.

[6] J. Hollomon and D. Turnbull, *Progress in Metal Physics*, vol. 4, pp. 333-388, 1953.

[7] D. Turnbull and R. Vonnegut, *Ind. Eng. Chem.,* vol. 44, p. 1292, 1952.

[8] B. Bramfitt, "The effect of Carbide and Nitride Additions on the Heterogeneous Nucleation Behaviour of Liquid Iron", *Metall. Trans.,* vol. 1, pp. 1987-1995, 1970.

[9] J. Reynolds and C.R. Tottle, *J. Inst. Metals,* vol. 80, p. 1328, 1951.

[10] A. Vertman and A.M. Samarin, *Dokl. Akad. Nauk SSSR,* vol. 134, p. 629, 1960.

[11] A. Samarin and V.A. Izmailov, *Sov. Phys. Dokl.,* vol. 14, p. 392, 1969.

[12] B. Lux, *Mod. Cast.,* vol. 45, pp. 222-232, 1964.

[13] D.M. Stefanescu, "Comparison between the Inoculation Efficiency of Sodium and Barium", *Giesserei- Prax.,* vol. 24, pp. 429-433, 1972.

[14] G. Sun and C.R. Loper, "Titanium Carbonitrides in Cast Iron", *AFS Trans.,* vol. 91, pp. 639-646, 1983.

[15] W. Weiss, "The Metallurgy of Cast Iron", in *B. Lux, I. Minkoff and F. Mollard, Ed. Georgi Publishing* , St. Saphorin, Switzerland, 1974.

[16] J. Wallace, *AFS Trans.,* vol. 83, pp. 363-378, 1975.

[17] L. De and Y.J. Xiang, *AFS Trans.,* vol. 99, pp. 701-712, 1991.

[18] M. Chisamera, I. Riposan and M. Barstow, "Paper 3," in *AFS International Inoculation Conference*, Rosemont (IL), 1998.

[19] A. Sommerfeld and B. Tonn, in *The Carl Loper Cast Iron Symposium*, Madison, WI, USA, 2009.

[20] I. Riposan, M. Chisamera, S. Stan, C. Hartung and D. White, in *The Carl Loper Cast Iron Symposium*, Madison, WI USA, 2009.

[21] M. Jacobs, T.J. Law, D.A. Melford and M.J. Stowell, *Metals Technology,* vol. 3, pp. 98-108, 1976.

[22] G. Sun and C.R. Loper, "Titanium Carbonitrides in Cast Iron", *AFS Trans.,* vol. 91, pp. 639-646, 1983.

[23] T. Skaland, O. Grong and T. Grong, “A Model for the Graphite Formation in Ductile Cast Iron”, *Metall. Trans A,* vol. 24A(10), pp. 2321-2345, 1993.

[24] D.M. Stefanescu, G. Alonso, P. Larrañaga, E. De la Fuente and R. Suarez, "A Comparative Study of Crystal Growth in Cast Iron and in Analogous Systems-Part I: Experimental Evidence of the crystallization of Graphite and of Analogous Cubic and Tetragonal Sytems", in *122nd MetalCasting Congress*, Fort Worth, Texas, 2018.

[25] E. Frás, M. Górny and H. López, *Metall. Mater. Trans. A,* vol. 38A, pp. 385-395, 2007.

[26] D. Bandyopadhyay, D.M. Stefanescu, I. Minkoff and S.K. Biswal, *in: G. Ohira, T. Kusakawa, E. Niyama (Eds), Physical Metallurgy of Cast Iron IV, Tokyo, Mat. Res. Soc. Proc.,* p. 27, 1989.

[27] S. Amini and R. Abbaschian, "Nucleation and Growth Kinetics of Graphene Layers from a Molten Phase, Carbon 51", pp. 110-123, 2013.

[28] D.M. Stefanescu, G. Alonso, P. Larrañaga, E. De la Fuente and R. Suarez, "On the Crystallization of Graphite from Liquid Iron-Carbon-Silicon Melts", *Acta Mater.,* vol. 107, pp. 102-126, 2016.

[29] B. Lux, I. Minkoff, F. Mollard and E. Thury, "Branching of Graphite Crystals growing from Metallic Solution”, in: B.Lux, I. Minkoff, F. Mollard (Eds), The Metallurgy of Cast Iron, Georgi Publishing Co., St Saphorin, Switzerland, pp. 495-508, 1975.

[30] D.M. Stefanescu, L. Dinescu, S. Craciun and M. Popescu, *Proc. 46th International Foundry Congress, CIATF, Spain,* vol. 37-1, 1979.

[31] M. Köning, M. Wessén and I. Svensson, *Proc. Modeling of Casting, Welding and Adv. Solidif. Proc. XII, Canada,* vol. 505-12, 2009.

[32] N. Aleksandrov, B.S. Milman, N.G. Osaka, L.V. Il'icheva and V.V. Vandreev, *Russian Castings Productions,* p. 365, 1975.

[33] E. Pan, K. Ogi and C.R. Loper, Jr, *Trans. AFS,* p. 509, 1982.

[34] G. Alonso, D.M. Stefanescu, P. Larrañaga and R. Suarez, «Understanding Compacted Graphite Iron Solidification Through Interrupted Solidification Experiments», *SPCI_X, 10-13th November, Argentina,* 2014.

[35] D.M. Stefanescu, G. Alonso, P. Larrañaga, E. De la Fuente and R. Suarez, "Reexamination of Crystal Growth Theory of Graphite in Iron-Carbon Alloys", Acta Materialia, vol. 139, pp. 109-121, 2017.

[36] K. Fang, "Atlas of the Morphology and Microstructure of the Graphite in Cast Iron", Science Publ. Co. of China, 2000.

[37] G. Purdy and M. Audier, "Electron Microscopical Observations of Graphite in Cast Irons", in: H. Fredriksson and M. Hillert (Eds.), The Physical Metallurgy of Cast Iron, Stockholm, Mat. Res. Soc. Symposia Proc., North-Holland, NY, pp. 13-23, 1985.

[38] T. Hara, T. Kitagawa, K. Kuroki, S. Saikawa, K. Terayama, S. Ikeno and K. Matsuda, "Morphologies of Some Graphites in Ductile Iron", *Material Trans. JIMM 55(9),* pp. 1500-1505, 2014.

[39] E. Ruiz, S. Alvarez and P. Alemany, *Phys. Review B*, vol. 49(11), pp. 7115-7123, 1994.

[40] P. Larrañaga, J.M. Gutiérrez, A. Loizaga, J. Sertucha and R. Suarez, *AFS Trans.*, vol. 112, pp. 547-561, 2008.

[41] G. Alonso, D.M. Stefanescu, P. Larrañaga, E. De la Fuente, R. Suarez, "On the Nucleation of Graphite in Lamellar Graphite Cast Iron", *AFS Trans.,* vol. 124, pp.205-213, 2016.

[42] P. Larrañaga, J. Sertucha, A. Loizaga, R. Suárez and D.M. Stefanescu, *AFS Trans.*, vol. 120, pp. 347-353, 2012.

[43] D.M. Stefanescu, G. Alonso, P. Larrañaga and R. Suarez, "On the Stable Eutectic Solidification of Iron-Carbon-Silicon Alloys", *Acta Materiala,* vol. 103, pp. 103-114, 2016.

[44] G. Alonso, D.M. Stefanescu, P. Larrañaga, E. De la Fuente, E. Aguado and R. Suarez, in *Advances in the Science and Engineering of Casting Solidification, L. Nastac*, B.C. Liu, H. Fredriksson, J. Lacaze, C.P. Hong et al. eds., Wiley TMS, pp.347-354, 2015.

[45] I. Riposan, M. Chisamera, S. Stan and T. Skaland, *Int. J. Cast Metals Res*., vol. 16 (1-3), pp. 105-111, 2003.

[46] G. Alonso, D.M. Stefanescu, P. Larrañaga and R. Suarez, "Graphite Nucleation in Compacted Graphite Cast Iron", *Keith Millis Symposium on Ductile Iron*, Hilton Head Island, South Caroline, USA, 2018.

[47] D.M. Stefanescu, G. Alonso, P. Larrañaga, E. De la Fuente and R. Suarez, "A Comparative Study of Cristal Growth in Cast Iron and in Analogous Systems - Part II: Experimental Work and the Multi-mechanism Theory of Graphite Crystallization", *122st Metalcasting Congress*, paper 18-032, Fort Worth, Texas, USA, 3-5th April, 2018.

[48] Y. Igarishi and S. Okada, *Int. J. Cast Metals Res.,* vol. 11, pp. 83-88, 1998.

[49] A. Vahed and D.A.R. Kay, *Metal Trans. B*, vol. 7B, pp. 375-383, 1976.

[50] B. Lia, K. Sim and R. Kim, "Effect of Sb-Ba-Ce-Si-Fe Post Inoculants on Microstructural and Mechanical Properties of As-Cast Pearlitic Ductile Iron", *Steel Research International*, 2019.

[51] B.B. Sangame and V.D. Shinde, "The Effect of Inoculation on Microstructure and Mechanical Properties of Ductile Iron", *IOSR Journal of Mechanical and Civil Engineering*, vol. 5, pp. 17-23, 2013.

[52] N.G. Kok, H. Sasaki, H. Kimura, T. Yoshikawa and M. Maeda, "Heterogeneous Nucleation of Graphite on Rare Earth Compounds during Solidification of Cast Iron", *ISIJ International*, vol. 58, pp. 123-131, 2018.

REZUMAT

Este unanim acceptat faptul că un control mai bun al formării grafitului în fonte este o soluție importantă pentru obținerea unor piese turnate cu proprietăți mecanice bune. Pe lângă grafitul rezidual care ar putea fi considerat un nucleant ideal pentru formarea grafitului în timpul solidificării, germinarea grafitului este direct legată de prezența unor incluziuni nemetalice formate în topitura de fontă. Aceste micro-incluziuni prezente în toate fontele turnate comerciale sunt în principal oxizi, silicați, sulfuri și nitruri, care par să acționeze ca germeni de nucleere pentru grafit atunci când satisfac anumite condiții specifice, incluzând o bună compatibilitate cristalografică, dimensiuni fine în topitură, stabilitate la temperaturi ridicate. Această cercetare și-a propus să clarifice unele dintre aceste ipoteze și să ofere argumente în acest sens în contextul multitudinii de opinii legate de germinarea grafitului. În acest scop, s-a efectuat o cercetare extinsă prin microscopie SEM asupra unei game extinse de probe obținute prin mai multe experimente de solidificare întreruptă pe fonte cu grafit nodular, compact și lamelar, cu și fără adaos de inoculanți comerciali. Natura incluziunilor cu rol de germeni de grafitizare a fost studiată prin utilizarea tehnicilor avansate de microscopie electronică (FEG-SEM), care a permis scanarea câmpului pentru obținerea spectrului de emisie, maparea și scanarea liniară. Au fost studiate detaliat efectele Ti si S și s-au efectuat calcule termodinamice de apreciere a abaterilor liniare și planare ale retelelor cristalografice ale compușilor lor fata de rețeaua grafitului pentru a evalua probabilitatea de formare a grafitului pe aceștia.

ABSTRACT

It is therefore assumable, that a better control of formation of graphite is an important approach to obtain soundness castings with good mechanical properties.In addition to the residual graphite which could be considered an ideal nucleant for the formation of graphite during solidification, the nucleation of this graphite is directly related to the presence of some non-metallic inclusions formed in molten iron. These micro-inclusions present in all commercial cast irons are mainly oxides, silicates, sulfides and nitrides, which seem to act as nucleation sites for graphite when they satisfy some specific conditions including good crystallographic, fine dispersion in the melt, low lattice disregistry and high stability at elevated temperatures. This investigation wants to clarify some of these assumptions and to provide some light in the convoluted world of the nucleation of graphite. With this purpose, an extensive SEM work was carried out on quenched samples, and several interrupted solidification experiments were conducted on spheroidal, compacted and lamellar graphite irons with and without addition of commercial inoculants. The nature of these inclusions was studied through the use of advanced Field Emission Gun scanning Electron Microscope (FEG-SEM) techniques, such as spectrums, mappings and line scan. The effect of titanium and sulfur was explored in depth through the use of irons were added in the base iron, and thermodynamic and disregistry calculations were carried out to evaluate the probability of formation of some of the nucleation sites.

CURRICULUM VITAE

PERSONAL INFORMATION Gorka Alonso

WORK EXPERIENCE

01/11/2006–Present Materials engineer

Fundación Azterlan, Durango (Spain)

Project Leader. Engineering, R&D and Metallurgical Processes Department. Structural development (mechanical calculation by finite elements) and solidification processes (process simulations). Responsible of extensiometry and fatigue tests carried out in fatigue bench (design of tools, planning, performance and tuning). Researcher of solidification processes of cast iron, developing projects whose results have been published in international conferences.

01/11/2005–01/11/2006 Materials engineer

Cie-Automotive, Berriz (Spain)

Scholarship by Fundación Novia Salcedo participating in a collaboration project between Cie Automotive and Maristas-Azterlan oriented to structural development, design and functional tests of automotive parts and compounds. The functions carried out were based on the 3D definition of different elements of assembly, performance of structural calculations by software of finite elements as well as definition of specifications of validation tests, tuning and performance of tests and analysis of results.

EDUCATION AND TRAINING

10/2014–Present

PhD student in the University of Transilvania in Brasov (Romania), in the materials engineering department, developing an important line of research in the field of nucleation and growth of graphite in ductile iron.

02/2005–06/2005

Course of **GRAPHIC REPRESENTATION IN MANUFACTURING MECHANICAL-CATIA V5** subsided by Basque Government. Fondo Formación Center (Barakaldo). Duration: 345h.

10/2004–12/2004

Course of **DESIGN AND MODIFICATION OF 2D AND 3D PLANS** subsided by Inem. IFES Center (Bilbao). Duration: 189h

03/2004–06/2004

Course of **GERMAN COMMERCIAL MANAGEMENT and GERMAN CUSTOMER SERVICE** subsided by Inem. F.P.Ibaiondo Center (Algorta). Duration: 418h

09/2003

Engineering of Materials by Escuela Superior de Ingenieros Bilbao (E.S.I.). Average score: 8.56

12/2002

Industrial Engineering by Escuela Superior de Ingenieros Bilbao (E.S.I). Average score: 7.010.